i-IDeA 2020
THE 5TH INTERNATIONAL INNOVATION, DESIGN AND ARTICULATION

UNIVERSITI TEKNOLOGI MARA
Cawangan Perlis
Kampus Arau

UiTM di hatiku

E-BOOK OF EXTENDED ABSTRACT

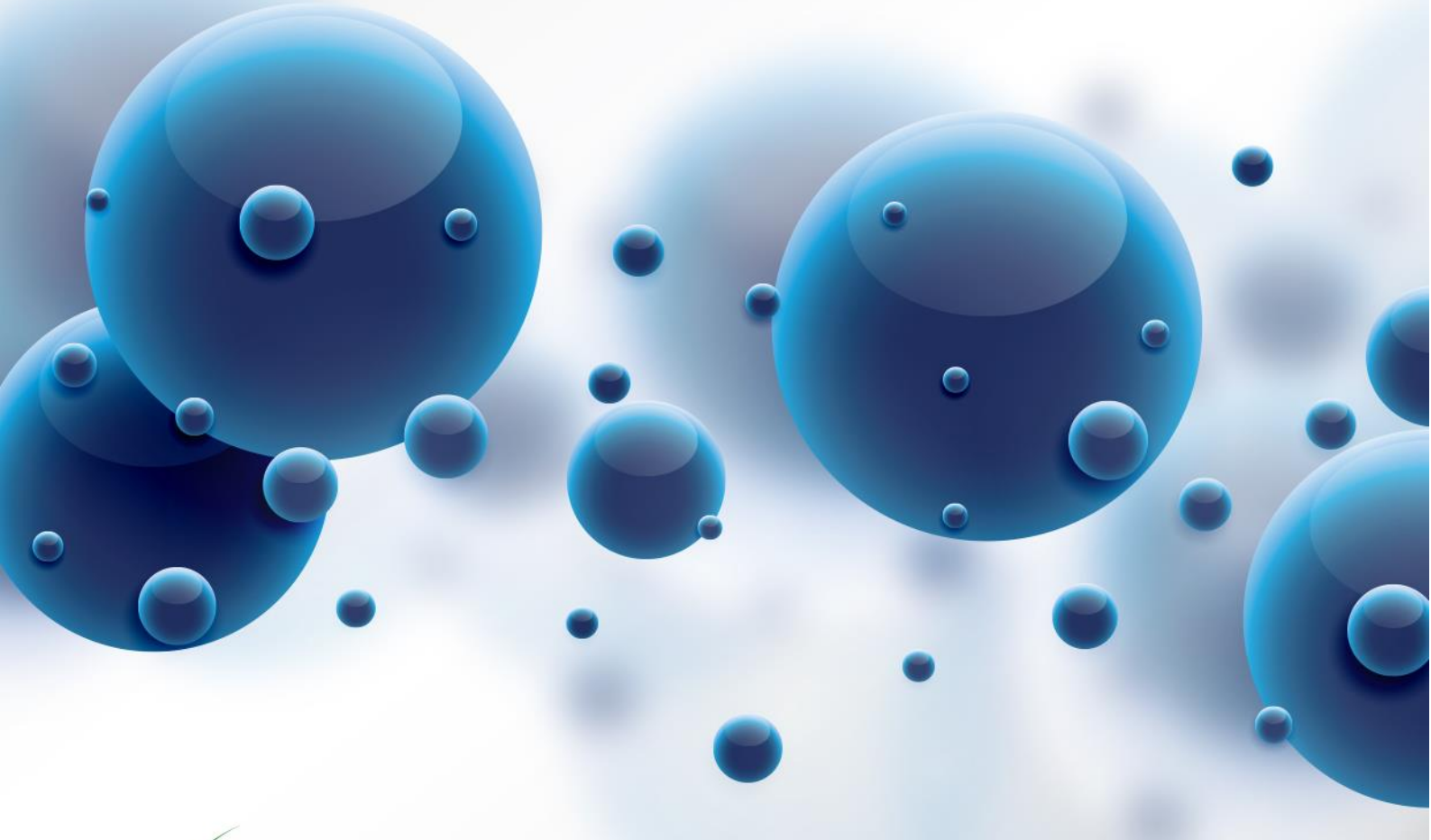

i-IDeA 4th ISTEC 2020
Exploring Materials for Future

INTERNATIONAL SCIENCES, TECHNOLOGY AND ENGINEERING CONFERENCE

DATE
8th OCTOBER 2020

VENUE
Virtual Conference via Google Meet

E-BOOK OF EXTENDED ABSTRACT

THE 4TH INTERNATIONAL SCIENCES, TECHNOLOGY AND ENGINEERING CONFERENCE (ISTEC 2020)

Copy Editors

Salamiah Zakaria

Nur Syazana Nazeri

Publisher

Research, Industrial Linkages, Community and alumni and Entrepreneurship (RICAEN), Universiti Teknologi MARA (UiTM) Perlis Branch,02600, Arau, Perlis.

Tel: 04-9882028/2296

Fax: 04-9882304

Perpustakaan Negara Malaysia
eISBN 978-967-16937-1-1

Perpustakaan Negara Malaysia Cataloging-in Publication Data

eISBN 978-967-16937-1-1

RICAEN,
The 4th International Sciences, Technology And Engineering Conference E-Book of Extended Abstract.

TABLE OF CONTENTS

TITLE	PAGES
EFFECT OF NiO Nps:BCZY RATIO ON THE MICROSTRUCTURE OF COMPOSITE ANODE	1
POTENTIAL OF SPENT BLEACH EARTH WASTE AS A GREEN BIODIESEL	4
SYNTHESIS AND CHARACTERIZATION OF HERBICIDE-4-CHLOROPHENOXYACETATE INTERLEAVED INTO LAYERED HYROXIDE SALT AND ITS CONTROL RELEASE STUDY	7
STUDY ON EPOXIDATION OF WASTE COOKING OIL: THE MECHANICAL AND THERMAL PROPERTIES IN POLYVINYL CHLORIDE FILMS	10
INVESTIGATION THE EFFECTS OF HNTS AND CNT NANOTUBES REINFORCED PMMA DENTURE BASE ON THE HARDNESS, IMPACT AND FLEXURAL STRENGTH	13
NUMERICAL SIMULATION ANALYSIS OF KENAF REINFORCED POLYPROPYLENE COMPOSITES	15
PERFORMANCE EVALUATION OF CLAM SHELLS AND COCKLE SHELLS AS SOURCE OF CALCIUM-BASED ADSORBENTS IN CARBON DIOXIDE ADSORPTION	18
PHYSICAL AND THERMAL PROPERTIES OF LOW ENERGY CONSUMPTION FIRED INDUSTRIAL WASTE-CLAY BRICKS FROM COCKLE SHELLS AND SODA LIME SILICA GLASS	21
CURE CHARACTERISTICS AND SWELLING BEHAVIOUR OF NaOH -TREATED PALM KERNEL SHELL (tPKS)/ ACRYLONITRILE RUBBER (NBR) COMPOUNDS	24
BIMETALLIC GOLD-COPPER NANOPARTICLES ON ANODIC ALUMINUM OXIDE (Au-Cu/AAO) MEMBRANE AS A CATALYST FOR REDUCTION OF p-NITROPHENOL	27
ENHANCING AROMATIC HYDROCARBON VIA CATALYTIC PYROLYSIS REACTION ON TORREFIED DEMINERALIZED PALM EMPTY FRUIT BUNCHES (TDPEFB)	30
$LaSrCoFeO_3$-Ba(Ce, Zr)O_3 NANOPARTICLES : SUPERIOR COMPOSITE CATHODE MATERIALS FOR PROTON CONDUCTING FUEL CELL APPLICATION	33
FISH GELATIN FILM INCORPORATED WITH LEMONGRASS EXTRACT FOR FRUIT WRAPPING APPLICATION	36
CHARACTERISATION ON GREEN COATING RESIN OF MALEINATED SOYBEAN OIL	39
FEASIBILITY OF BANANA PEELS AND SUGARCANE BAGASSE AS ECO-FRIENDLY LOST CIRCULATION MATERIAL ADDITIVES IN DRILLING MUD APPLICATION	42
ELECTRICAL PERFORMANCE OF $La_{0.6}Sr_{0.4}Co_{0.2}Fe_{0.8}O_{3-\delta}$ MODIFIED WITH LESS REDUCIBLE CATION	45

OPTICAL, STRUCTURAL AND MORPHOLOGICAL PROPERTIES OF SiO_2-ZrO_2: Er^{3+}/Yb^{3+} THIN FILM DEPOSITED ON FUSED SILICA AND SILICON WAFER SUBSTRATE 48

REMOVAL OF LEAD FROM AQUEOUS SOLUTION by TREATED SUGARCANE BAGASSE 51

PREPARATION AND CHARACTERIZATION OF *CAULERPA RACEMOSA* REINFORCED CORN STARCH BIODEGRADABLE FILM 54

International Science, Technology and Engineering Conference, (ISTEC 2020) 1-3
e-isbn: 978 -967- 16937-1-1

EFFECT OF NiO Nps:BCZY RATIO ON THE MICROSTRUCTURE OF COMPOSITE ANODE

*Noor Hidayah Aniza Zakaria[1], Hanani Yazid[2] and Nafisah Osman[2]
[1]*Proton Conducting Fuel Cell Group, Faculty of Applied Sciences, Universiti Teknologi MARA, 40450 Shah Alam, Selangor,Malaysia.*
[2]*Faculty of Applied Sciences, Universiti Teknologi MARA, 02600 Arau, Perlis, Malaysia.*
*hidayah_aniza@yahoo.com

PURPOSE/AIM & BACKGROUND

Nickel (Ni) is the most popular catalyst that has been used as an electronic conductor in fuel cell due to its natural porosity and lower cost compared to platinum (Pt). NiO-$Ba(Ce,Zr)O_3$ is one of promising cermet that has been used as composite anode in proton conducting fuel cell (PCFC) application. Nowadays, researchers are moving towards nanotechnology and eventually replaced the coarse nickel oxide (NiO) in anode side to nickel oxide nanoparticles (NiO Nps). The nanostructure of NiO Nps can promote higher number of active site and increase the performance of the PCFC. In the other hand, composition ratio between electronic conductor (Ni) to ceramic also play important role for the anode performance.Different ratios of NiO to $Ba(Ce,Zr)O_3$ will create different microstructure and porosity that effect the performance of the material (Abdalla, 2018; Zakaria, 2019). In this work, NiO Nps-BCZY with two different composition ratios (50:50 and 60:40) were prepared using mixing method and then characterized by scanning electron microscopy (SEM/ EDX) and X-ray diffractometer (XRD). Structural analysis confirmed that a high phase of cubic structure of NiO Nps-BCZY was obtained without the existence of any secondary phase for ratio 60:40. However, for ratio 50:50, secondary phases of $BaCeO_3$ and $BaZrO_3$ were observed represented that the NiO Nps-BCZY cermet were not completely formed. Morphological observation showed the NiO nanoparticles embedded in NiO Nps-BCZY were spherical in-shape for both of the ratios. The NiO Nps-BCZY particles tend to form agglomerates with the size 50 to 300 nm.

METHODOLOGY

NiO Nps-BCZY composite anode powder was prepared by a sol-gel method using NiO Nps and BCZY powders (BCZY = $BaCe_{0.54}Zr_{0.36}Y_{0.1}O_{2.95}$). To prepare NiO nanoparticles powder, stoichiometric amount of nickel nitrate hexahydrate, $Ni(NO_3)_2.6H_2O$ (99%, Acros) and citric acid monohydrate (CA), $C_6H_8O_7H_2O$ (99.5%, MERCK) were dissolved in deionized water in two different beakers and the Ni nitrate solution then was dripped into CA solution under stirring condition with mol ratio of citric acid to nickel nitrate, (C/N) = 1. The homogeneous mixture was gradually heated until 70 ^oC for 2 hours and subjected to drying process using an oven at 80 ^oC for 24 hours. The mixture was grinded and calcined at 450 ^oC for 2 hours with heating rate 5 ^oC/min (Wu, 2007; Zorkipli, 2016). The synthesis method for BCZY powder was followed as previously reported by Samat (2016) and Zakaria (2019) . NiO Nps-BCZY composite anode powder was prepared using a mixing method. The respective NiO Nps powder and BCZY powder with weight ratio of 50:50 (NiO:BCZY) was grinded with ethanol, C_2H_5OH (95.1%, MERCK) for an hour. The mixture was stirred for 2 hours on a hotplate and subjected to drying process at 85 ^oC for 12 hours (Mehran, 2018). The powder was grinded and calcined at 1100 ^oC (6 hours) to obtain NiO Nps-BCZY composite anode.The morphology and structural analysis of NiO Nps-BCZY composite anode powders (50:50 and 60:40) was observed using respective scanning electron microscope (SEM), Benchtop Phenom XL with 7000x magnifications, and X-ray diffractometer (XRD), XRD 6000 Shimadzu.

FINDINGS/RESULTS

Figure 1 presents the SEM micrograph of 50:50 composite anode powder with EDX mapping. It can clearly seen that the particles of the anode powder was clumping together lead to bigger size of

particles. The strong nuclei attraction between the particles was due to high surface area (contributed by nano-sized NiO and fine BCZY powder) and eventually causing the agglomerations of particles. 50:50 and 60:40 composite anode powder, the particle size was the same which in the range of 50 to 300 nm.

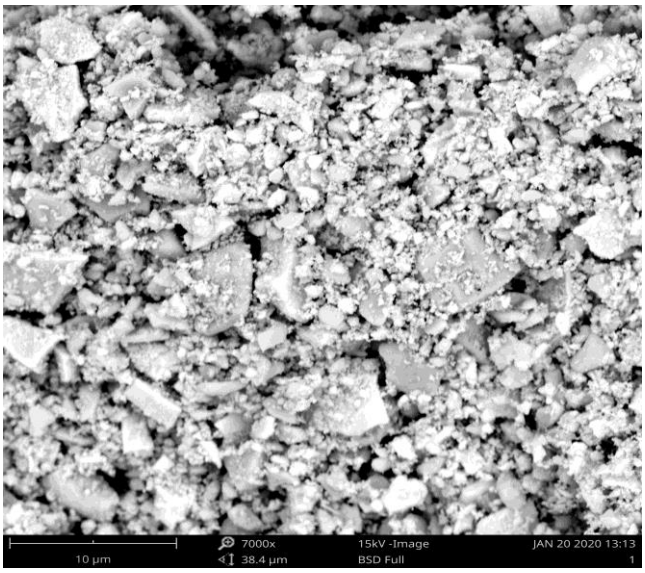

Figure 1. SEM image of NiO Nps-BCZY Composite Anode (50:50)

Figure 2 shows the EDX spectrum of 50:50 composite anode powder. There were three intense peaks that presenting Ni element, and two sharp peaks of Ce element. The result was in agreement with structural analysis (XRD analysis). In addition, XRD analyses showed the composite anode with ratio 50:50 formed secondary phase of barium cerate ($BaCeO_3$, JCPDS 82-2486) and barium zirconate ($BaZrO_3$, JCPDS 89-2486).

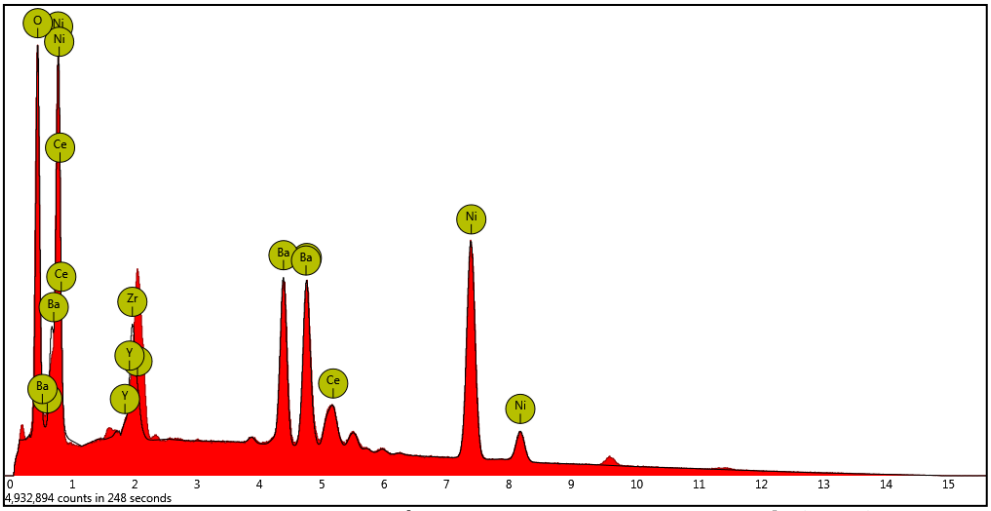

Figure 2. EDX Spectrum of NiO Nps-BCZY Composite Anode (50:50)

CONCLUSIONS

The NiO Nps-BCZY composite anode powders with weight ratio of 50:50 and 60:40 were synthesized using a sol-gel method assisted with mixing process. Only the NiO Nps-BCZY powder with composition 60:40 was confirmed as a composite anode as it presented two phases of NiO (JCPDS 01-1239) and BCZY (JCPDS 89-2485. Whereas, NiO Nps-BCZY with composition 50:50 formed secondary phase of barium zirconate ($BaZrO_3$) and barium cerate ($BaCeO_3$). Nevertheless, the particle size for both composition was in the range 50 to 300 nm. Further works on the electrical performance

of NiO Nps-BCZY composite anode are in progress and will be reported elsewhere.

ACKNOWLEDGEMENT
This work is supported by Ministry of Education (MOE) Malaysia via Grant 600-IRMI/FRGS 5/3 (119/2019). The authors thank Universiti Teknologi MARA (UiTM) for the facilities and support provided.

REFERENCES

A.A. Samat, M.R. Somalu, O.H. Hassan and N. Osman. (2016). LSC cathode prepared by polymeric complextion method for proton-conducting SOFC application. *J. Euro. Cer. Society*, 25, 382-393.

A.M. Abdalla, S. Hossain, A.T. Azad, P.M.I. Petra, F. Begum, S.G. Eriksson and A.K. Azad. (2018). Nanomaterials for solid oxide fuel cells: A review, Renew. and Sustain. *Energy Rev*., 82, 353-368.

M.T. Mehran, M.Z. Khan, S.B. Lee, T.H. Lim, S. Park and R.H. Song. (2018). Improving sulfur tolerance of Ni-YSZ anodes of solid oxide fuel cells by optimization of microstructure and operating conditions. *Int. J. of Hydrogen Energy*, 43, 1202-11213.

N.H.A Zakaria, N.S.M. Affandi, A.N. Zainon, H. Yazid and N. Osman. (2019). Electrical conductivity of anode supported NiO-BCZY|BCZY|LSCF-BCZY button cell at intermediate temperatures. *JSSST*, 27,15-21.

N.N.M. Zorkipli, N.H.M. Kaus and A.A. Mohamad. (2016). Synthesis of NiO nanoparticles through sol-gel method. *Procedia Chem*, 19, 626-631.

Y. Wu, Y. He, T. Wu, T. Chen, W. Weng and H. Wan. (2007). Influence of some Parameters on the Synthesis of Nanosized NiO Material by Modified Sol-gel Method. *Materials letters*, 61, 3174-3178.

***Keywords*:** NiO nanoparticles, composite anode ratio, proton conducting.

International Science, Technology and Engineering Conference, (ISTEC 2020) 4-6
e-isbn: 978 -967- 16937-1-1

POTENTIAL OF SPENT BLEACH EARTH WASTE AS A GREEN BIODIESEL

*Asnida Yanti Ani[1,2], Muhammad Luqman Md Ali[1,2] , Nur Syazlinda Esa' Ayuddi[1],
Nur Nasulhah Kasim[1,2], Khudzir Ismail[1,2], and Mohd Azlan Mohd Ishak[1,2]

[1]*Faculty of Applied Sciences, Universiti Teknologi MARA, Perlis Branch, Arau Campus, 02600, Arau, Perlis, Malaysia.*

[2]*Fuel & Biomass Energy Research Group, Universiti Teknologi MARA, Perlis Branch, Arau Campus, 02600, Arau, Perlis, Malaysia.*

*asnida933@uitm.edu.my

PURPOSE/AIM & BACKGROUND

Biodiesel has received special attention in the last years due to its potential for replacing conventional diesel fuel (Plata., 2020) in transportation and household appliances as they are expected to be decrease in near future (Gui et al., 2008). Bio-energy from biomass and waste when converted to biodiesel can become reliable substitutes to replace fossil fuels. They give benefits in terms of biodegradability, renewability, nontoxic and lower emission into environment (Zheng et al., 2012). One of the highlighted wastes is Spent Bleaching Earth Waste (SBEW), a by-product material derived from vegetable oil refining industry. It is used in bleaching process to eliminate harmful components, strong odor or colored compounds in the raw materials of vegetable oils (Boukerroui & Ouali, 2000; Wafti et al., 2011) Oil from this resource is non-edible as it contains components that are toxic to human body (Kumar & Sharma, 2011). Meanwhile, open disposal of SBEW creates fire hazard and threat to environment which makes it necessary for the regeneration of oil in the SBEW. Conventional extraction methods to recover oil in SBE uses a lot of solvents and catalysts. Hence, it lead to the discovery of new solvent called deep eutectic solvent (DES) which works as catalyst or co-solvent in biodiesel synthesis and as extracting solvent in biodiesel purification step (Troter et al., 2016). DESs is said able to improve the catalytic abilities, avoid saponification and has higher efficiency in separation and purification processes (Troter et al., 2016). Through this study, in-situ esterification method was chosen as it is believed that there's potential in enhance the reaction rate and lowering the reaction time. Moreover the effect of the following reaction parameters was studied: a) effect of reaction time and b) DES:Methanol volume ratio. This study aims to produce biodiesel by in situ transesterification of SBE with the aid of DESs as media.

METHODOLOGY

Spent bleaching earth waste (SBEW) acquired from Eco Oils (Negeri Sembilan) Sdn. Bhd was dried in the oven at 107 ± 2 ^{o}C for 24 hours. Choline chloride (ChCl) was mixed with ethylene glycol (EG) at 1:2 molar. The mixture was stirred at 300 rpm and 80 ^{o}C for 1 h until homogenous and transparent liquid was obtained. The in-situ reaction was carried out by reflux at 65 ^{o}C between 80-160 min with continuous stirring of 25 g SBE (at oil content 18 wt. %) to give 5 mL/g of solvent to SBEW ratio. The DES to methanol volume ratio was varying from 5-25%. After the reaction stopped, the sample was centrifuged for 5 min at 1000 rpm to separate the solid-liquid mixture. Then, the extracted liquid was transferred into separating funnel and stand for 1 hour. The bottom layer containing glycerol, methanol and DES was removed before adding equal amount of hexane and distilled water to remove excess methanol. The hexane which contained FAME was evaporated using rotary evaporator and pure FAME was obtained. The weight of crude oil was weighed, and the biodiesel yield was determined. FAME yield was analyzed using GC-FID by dissolving 100 mg of crude biodiesel in 1 mL of 0.6 mg/mL methyl heptadecanoate internal standard. Then 1µl of sample was injected into oven to allow detection of FAME in sample. The programmed temperature was set as follow: initial column temperature was maintained for at 190 ^{o}C for 5 min, and then elevated by 5 ^{o}C/min to 230 ^{o}C remained for 5 min. The FAME yield was calculated using Equation 1 based on Gu et al., (2015).

$$\text{Yield}_{\mathbf{FAME}}\,\% = \sum \frac{A - A_{IS}}{A_{IS}} \times \frac{(C_{IS} \times V_{IS})}{m} \times 100 \qquad \text{(Eqn 1)}$$

Where, $\sum A$ = total peak area of FAME, A_{IS} = peak area of methyl heptadecanoate, m = mass of sample (mg), C_{IS} = concentration of internal standard (mg/mL), and V_{IS} = volume of internal standard (mL)

FINDINGS/RESULTS

Effect of Reaction Time on Crude Yield, FAME Yield, and FFA Content

Reaction time plays significant roles in various reaction prior to provide sufficient time toward completion of reaction. The reaction time tested in this study ranged from 80-160 min. From laboratory experiment, the result shows as the reaction time increased, crude yield increased until it reaches highest yield at 140 min (see Figure 1). Reaction time above 140 min led to no further increment of biodiesel yield. Hence, it is the optimum reaction time for in-situ esterification of SBE sample. This shows that the loading of DES as the catalyst with sufficient contact time improved the conversion of biodiesel. In addition, the highest FAME yield was obtained at 140 min with 89.78% of purity shows DES also helps in increasing the FAME yield. It was observed that the FFA content reduced with a function of time (see Figure 1). The FFA content reduced from 1.04% at the first 80 minutes to 0.84% after the completion at 160 minutes. This indicates that the longer the reaction time, it provides longer interaction time between the crude biodiesel and the DES. Overall result shows that under the presence of DES, FFA content of biodiesel is lower than 2%. compared with the raw SBEW oil at 13.93% FFA. This is due to hydrogen bonding between DES and hydroxyl group of FFA where these compounds were extracted out and lowered FFA content of biodiesel. The biodiesel is separated out into another layer since it does not have hydroxyl group. Apart from FFA, DES also extracted out other impurities such as monoglycerides, diglycerides, water, and residual methanol through interaction with choline chloride as the hydrogen bond acceptor (HBA) and ethylene glycol as hydrogen bond donor (HBD) by formation of hydrogen bonding (Niawanti et al., 2017).

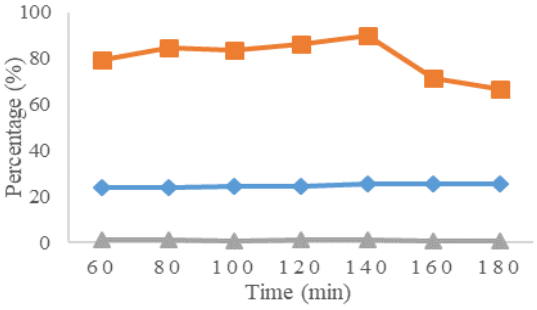

Figure 1. Effect of reaction time on percentages of crude biodiesel yield, FAME yield and FFA content at 15% DES/MeOH (v/v%) and 65 ºC temperature.

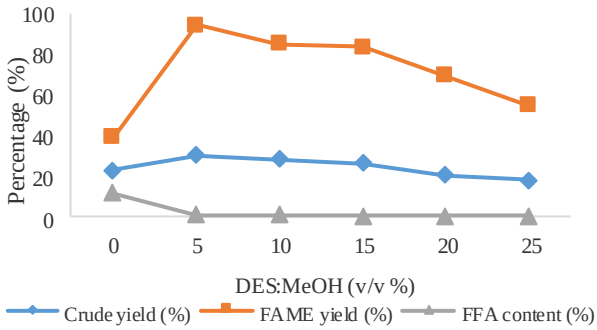

Figure 2. Effect of DES:MeOH (v/v %) on percentages of crude biodiesel yield, FAME yield and FFA content at 15% DES/MeOH (v/v%) and 65 ºC temperature.

Effect of DES to Methanol Ratio (vol %) on Crude Yield and FFA Content

In the present work, the DES (ChCl:EG) played the roles as catalyst and co-solvent. Since this type of reaction is solid-liquid reaction, the contact area between the oil-bearing material of SBE and catalyst was the key to the esterification reaction. From figure 2, the highest yield of crude biodiesel was achieved at 5% v/v DES:MeOH with crude and FAME yield of 30.26% and 94.64% respectively. Further increment in ratio shows declining trends in both crude and FAME yield. Tarigan et al., (2017) stated that products may adsorbed on catalyst if the amount of catalyst too high and therefore leading to decrease in end yield. Excess glycerol molecules in DES may attract methanol molecules and bind to them which leads to less availability of free methanol molecules for reaction when DES ratio is too high (Gu, Huang, Tang, Tian, & Zhang, 2015).

Physicochemical properties of biodiesel

The properties of SBEW biodiesel produced from the in-situ process was studies and the result were compared to standard biodiesel properties of ASTM and EN. The results are summarized in Table 1. From the data, it can be concluded that the biodiesel met the required criteria.

Table 1: Physicochemical Properties of biodiesel.

Specification	This Study	Biodiesel Standard	
		EN 14214	ASTM D6751
Density at 25 ^{o}C (g/cm^{3})	0.89	0.86-0.90	-
Kinematic viscosity at 40 ^{o}C (mm^{2}/s)	4.1	3.5-5.0	1.9-6.9
Acid value (mg KOH/g)	0.31	0.5 max	0.5 max

CONCLUSIONS

SBEW which is considered as a non-valuable and caused environmental problems are now has the potential as a feedstock of biodiesel production. The introduction of DES as catalyst and co-solvent during in-situ esterification shorten reaction time as the extraction and transesterification processes occur simultaneously. The physicochemical analysis on the biodiesel produced falls within the acceptable range in accordance to ASTMD6751 and EN 14214.

REFERENCES

Boukerroui, A., & Ouali, M. S. (2000). Regeneration of a spent bleaching earth and its reuse in the refining of an edible oil. *Journal of Chemical Technology and Biotechnology*, *75*(9), 773–776.

Gu, L., Huang, W., Tang, S., Tian, S., & Zhang, X. (2015). A novel deep eutectic solvent for biodiesel preparation using a homogeneous base catalyst. *Chemical Engineering Journal*, *259*, 647–652.

Gui, M. M., Lee, K. T., & Bhatia, S. (2008). Feasibility of edible oil vs. non-edible oil vs. waste edible oil as biodiesel feedstock. *Energy*, *33*(11), 1646–1653.

Kumar, A., & Sharma, S. (2011). Potential non-edible oil resources as biodiesel feedstock: An Indian perspective. *Renewable and Sustainable Energy Reviews*, *15*(4), 1791–1800.

Niawanti, H., Zullaikah, S., & Rachimoellah, M. (2017). Purification of biodiesel by choline chloride based deep eutectic solvent. *AIP Conference Proceedings*, *1840*.

Plata, V., Rojas, O., & Gauthier-Maradei, P. (2020). Improvement of palm oil biodiesel filterability by treatment with reactivated spent bleaching earths, *Fuel* ,260, 116198.

Tarigan, J. B., Prakoso, H. T., Siahaan, D., & Kaban, J. (2017). Rapid Biodiesel Production from Palm Kernel through In Situ Transesterification Reaction Using CaO as Catalyst. *International Journal of Applied Chemistry*, *13*(3), 631–646.

Troter, D. Z., Todorovi, Z. B., Đokic-Stojanovic, D. R., Stamenkovi, O. S., & Veljkovi, V. B. (2016). Application of ionic liquids and deep eutectic solvents in biodiesel production : A review. *Renewable and Sustainable Energy Reviews*, *61*, 473–500.

Wafti, N. S. A., Yoo, C. K., Lin, S. W., Yaw, T. C. S., & Abdullah, L. C. (2011). Deoiling efficiency for oil extraction from spent bleaching clay and the quality of recovered oil. *Journal of Oil Palm Research*., 23, 1005-1010.

Zheng, L., Li, Q., Zhang, J., & Yu, Z. (2012). Double the biodiesel yield: Rearing black soldier fly larvae, Hermetia illucens, on solid residual fraction of restaurant waste after grease extraction for biodiesel production. *Renewable Energy*, *41*, 75–79.

Keywords**:** *In-situ transesterification; SBEW; Biodiesel; waste; DES*

International Science, Technology and Engineering Conference, (ISTEC 2020) 7-9
e-isbn: 978 -967- 16937-1-1

SYNTHESIS AND CHARACTERIZATION OF HERBICIDE-4-CHLOROPHENOXYACETATE INTERLEAVED INTO LAYERED HYROXIDE SALT AND ITS CONTROL RELEASE STUDY

Farah Liyana Bohari, Fardzil Idham Sufian , *Sheikh Ahmad Izaddin Sheikh Mohd Ghazali and Nur Nadia Dzulkifli

Faculty of Applied Sciences, Universiti Teknologi MARA, Negeri Sembilan branch, Kuala Pilah campus, 72000 Kuala Pilah, Negeri Sembilan, Malaysia,

**sheikhahmadizaddin@uitm.edu.my*

PURPOSE/AIM & BACKGROUND

The aim of this paper is to synthesise the layered hydroxide salt (LHS) especially in the layered zinc hydroxide (LZH) category, interleaved with the herbicide called 4-chlorophenoxyacetic acid (4CPA) and this has successfully been done to form layered zinc hydroxide-4CPA (Z4CPA) nanohybrid. The nanohybrid can help reduce the environmental impacts caused by the higher concentration of common herbicides as the system controls the delivery rate of the agrochemicals. Herbicides are well known in agriculture to kill unwanted plants such as weeds that infest the plant crops and reduce the marketability of the agriculture production. However, a high dosage of herbicide may affect the soil quality and the water drainage system in the ground which flows to nearby water sources (Derylo-Marczewska et al., 2017). High acidity from an increased dosage of herbicide will cause water pollution that will harm humans and the aquatic life. Thus, the synthesised nanohybrid can help reduce the problem by altering the delivery rate of the herbicide to the environment when applying it to the field crops. The delivery system mentioned was called the control release system and it can be utilized by interleaving the herbicide with an inorganic material called the layered metal hydroxide. Layered metal hydroxide is a 2-dimensional nanosheet stacked on top of one another (Mishra *et al.*, 2018). It has a positive net charge while the interlayer domain between the two nanosheets was dominated with negative ions or anions. The cation used here is the divalent zinc cation which will become the layered hydroxide salt known as zinc layered hydroxide (Adam *et al*., 2018; Ahmad *et al*., 2016). The general chemical formula for the layered zinc hydroxide is $M^{2+}(OH)_{2-x}(A^{m-})_{x/m}{\cdot}nH_2O$ in which M^{2+} is the metal cation Zn^{2+} while A^{m-} is for the counter anion which is 4CPA (Hussein *et al.*, 2012). In this research, the successful interleaved product of 4CPA into LHS results in a nanomaterial namely, Z4CPA which is cheap and environmental-friendly to fight against weeds. The anion can be introduced between the interlayer of LHS via the ion exchange or coprecipitation methods while hydrothermal treatment was used to enhance the crystallinity of the products. Additionally, the slow release of 4CPA from the LHS in the selected aqueous media has also been examined in this research.

METHODOLOGY

Synthesis of LHS Interleaved with 4CPA

All of these solutions were prepared using deionized water. 0.1 M 4CPA was added into 0.05 M of zinc oxide in a 250 ml conical flask. Then, the slow addition of 2 M of sodium hydroxide was added to the solution and the pH was adjusted to about 7±0.5 under vigorous stirring for 3 hours. Next, the homogenized solution was placed inside an oil bath shaker set at 70°C for 18 hours to undergo aging process. The solvent was decanted and the remaining was centrifuged. Later, 30 ml of deionized water was added into the tube to resuspend the precipitate into the teflon autoclave for hydrothermal treatment for 1 hour at 120 °C. The solution was centrifuged and washed with deionized water for three times. The sample was dried in an oven at 70 °C for 24 hours. Lastly, the sample was grounded into fine powder for further characterization with the PXRD, FTIR, FESEM-EDX and BET analyses.

Controlled Release Study

Firstly, the maximum wavelength of the 4CPA must be identified by running the 4CPA solution against a blank sample in the wavelength range set from 200-600 nm. After the maximum wavelength of the 4CPA had been identified, the control release study had been conducted using the kinetics system of the UV-Vis spectroscopy. Later, the 100 % release of Z4CPA has been done inside the quartz cuvette by using 0.25 mg of the sample to be added into 2M HCl solution. The wavelength was set according to the maximum wavelength of the 4CPA to be run for 360 minutes. Afterwards, the control release of Z4CPA was studied in variety of media solutions of sodium chloride, sodium carbonate and sodium phosphate at concentration of 0.01 M each. Next, around 0.25 g of Z4CPA sample was inserted inside the quartz cuvette containing the media solution and the control release was investigated in a timeframe of 360 minutes by using the UV-Vis Spectroscopy.

FINDINGS/RESULTS

X-Ray Diffraction

The diffractograms for the 4CPA, ZnO and the layered metal hydroxide of Z4CPA was obtained from the analysis of the powder X-ray diffraction analysis as shown in figure 1. In the PXRD patterns, figure 1(b) denotes the zinc oxide that consisted of five peaks in between the range of 30° to 60°. The ZnO diffractogram obtained from the PXRD analysis shows the presence of all five peaks which means that the ZnO was of a pure phase that exhibited high crystallinity (Adam *et al*., 2018; Ahmad *et al*., 2016). The ZnO will react directly with 4CPA under aqueous medium to become the Z4CPA. In the synthesized nanohybrids shown in figure 1(c), it was found out that the basal spacing at 2θ of 4.0815 degrees was 21.6 Å from the calculation using Bragg's law. This peak is important as the existence of the peak between the range of 0° to 10° indicates that the interleave possibly occurred between the host and the anion.

CONCLUSIONS

In conclusion, the conducted study has successfully achieved the overall objectives. Based on the PXRD analysis, interleaving was confirmed by the expansion of the basal spacing at 21.6 Å, which indicates the interlayer space has significant changes in terms of height. Moreover, the spatial orientation of 4CPA in the LHS interlayer proposed was 11.6 Å according to the basal spacing of 21.6 Å. Next, the ATR-FTIR spectroscopy has proven that significant bands such as in the 4CPA can be observed in the spectrum of Z4CPA. However, there was a slight shift in the wavenumber due to the modification of the 4CPA natural frequency post-interleaved. The analysis of BET using the nitrogen-desorption isotherms shows that the synthesized nanohybrid of the Z4CPA was a mesoporous material. Meanwhile, the findings from FESEM-EDX exhibits the ZnO with irregular granular structure has transformed into non-uniform flaky shapes with no specific structures of the Z4CPA. Last but not least, the study effects of the Z4CPA to be an eco-friendly nanocarriers in the herbicidal agriculture has also achieved its objective. The control release mechanism of the Z4CPA was performed using the UV-Vis Spectroscopy kinetic modes and the result has shown satisfactory as the release profiles of the anion 4CPA from the LHS matrices has increased with the contact time followed by a steady release. Additionally, the anions saturated release was in the order of phosphate > carbonate > chloride with percentages release of 90%, 75%, 50%, respectively.

REFERENCES

Derylo-Marczewska, A., Blachnio, M., Marczewski, A. W., Swiatkowski, A., & Buczek, B. (2017). Adsorption of chlorophenoxy pesticides on activated carbon with gradually removed external particle layers. *Chemical Engineering Journal*, *308*(1), 408–418.

Mishra, G., Dash, B., & Pandey, S. (2018). Layered double hydroxides: A brief review from fundamentals to application as evolving biomaterials. *Applied Clay Science*, *153*(June 2017), 172–186.

Hussein, M. Z., Rahman, N. S. S. A., Sarijo, S. H., & Zainal, Z. (2012). Herbicide-intercalated zinc layered hydroxide nanohybrid for a dual-guest controlled release formulation. *International Journal of Molecular Sciences*, *13*(6), 7328–7342.

Adam, N., Ahmad, S., Sheikh, I., Ghazali, M., Dzulkifli, N. N., & Jamion, N. A. (2018). Synthesis and Physiochemical Properties of Zinc Layered. *International Journal of Engineering & Technology*, *7*(January), 49–51.

Ahmad, R., Hussein, M. Z., Sarijo, S. H., Rasidah, W., Abdul, W., & Hin, T. Y. (2016). Synthesis and Characteristics of Valeric Acid-Zinc Layered Hydroxide Intercalation Material for Insect Pheromone Controlled Release Formulation. *Journal of Materials*, *2016*, 9.

***Keywords*:** Layered Zinc Hydroxide (LZH); 4-Chlorophenoxyacetic Acid (4-CPA); interleaved; hydrothermal; control release

International Science, Technology and Engineering Conference, (ISTEC 2020) 10-12
e-isbn: 978 -967- 16937-1-1

STUDY ON EPOXIDATION OF WASTE COOKING OIL: THE MECHANICAL AND THERMAL PROPERTIES IN POLYVINYL CHLORIDE FILMS

*Farhana Othman, Nur Artiqah Musaa and Muhamad Faris Mohamed Ariffin
Universiti Teknologi MARA Perlis Branch, 02600 Arau, Perlis, Malaysia,
*farhana2876@uitm.edu.my

PURPOSE/AIM & BACKGROUND

Epoxidized waste cooking oil methyl ester (EWCO-ME), an alternative bio-based plasticizer is identified as a potential substitution for toxic petroleum-based phthalates in polyvinyl chloride (PVC) film. EWCO-ME was synthesized via in-situ epoxidation reaction between formic acid (HCOOH) and hydrogen peroxide (H_2O_2), and it was applied as a primary plasticizer in PVC films formulation. In this study, the main objectives were to determine the oxirane oxygen content (OOC) and relative conversion oxirane (RCO) at different molar ratio which were 0.05:2.2 and 0.6:1.7; secondly, the effect of ratio EWCO-ME on mechanical properties and the glass transition temperature (T_g) of EWCO-ME/PVC formulation were studied.

Epoxidized edible vegetable oils (such as soybean, linseed, sunflower and rubber seeds) are one of the most currently studied PVC plasticizers since it is renewable sources (Chen et al., 2015). However, the unreacted double bonds in epoxidized vegetable oils reduce compatibility between PVC and the plasticizer, and thus epoxidized oils are commonly applied either as a secondary plasticizer or combined with other additives (Yang et al., 2017). Hence, high conversion of the double bonds into oxirane rings (such as epoxy groups) is a desirable characteristic in the production of high quality epoxidized oil-based plasticizers.

METHODOLOGY

Materials

The reagents employed in this study were: waste cooking oil, collected from food stalls near UiTM Arau, Perlis; chemicals all acquired from Merck, Malaysia; and PVC resin supplied by Kaneka, Malaysia.

Synthesis of Waste Cooking Oil-Methyl Ester (WCO-ME)

In the first step of acid esterification was took place. In the second step of transesterification, 229 g esterified WCO and methanol by using molar ratio methanol to WCO (12:1) were placed in a flask with a stirrer, a reflux condenser and a thermometer, followed by stirring at 600 rpm, 65 °C for 3 h catalyzed with 1% v/v sodium hydroxide. The excess glycerol was removed, and crude biodiesel WCO-ME was collected. Then, the mixture was washed twice with 80 °C distilled water (Silva et al., 2011).

Synthesis of Epoxidized Waste Cooking Oil-Methyl Ester (EWCO-ME)

Initially, the epoxidation reaction molar ratio of 0.05:2.2 (HCOOH: H_2O_2) was set up. A 20 g of WCO-ME and 5 g of HCOOH were added to a flask with magnetic stirring, and the mixture was maintained at 60 °C. Then, 220 g of H_2O_2 (30% v/v) was added drop wise for 30 minutes, and the mixture was continuously stirred for 4 hours. The mixture allowed to cool at room temperature and maintained to pH 7. The reaction was repeated with 0.6:1.5 molar ratio (Vaibhav et al., 2006). In order to determine oxirane oxygen content (OOC), iodine value (IV) was measured by Wijs method from ASTM D1959. OOC value was determined by direct method using 0.1 N hydrobromic acid solution in glacial acetic acid with some modification (ASTM D1652 and D2074) (Kousaalya et al., 2018).

Preparatıon of PVC Films

PVC resin powder (0.4 g) was mixed with 9 mL THF, followed by the addition of synthesized EWCO-ME; no thermal stabilizers were utilized. The mixture was thoroughly agitated until it is transparent

and homogeneous sample solution. Then, the solutions were cast into 10 cm diameter glass petri dishes, and the solvent was evaporated at ambient temperature (Jia et al., 2015). The composition of plasticizer for preparing PVC films were PVC-10, PVC-20, PVC-30 and PVC-40 based on w/w% plasticizer. The films were characterized using Differentil Scanning Calorimetry (DSC) analsysis and Instron Tensile Testing Machine.

FINDINGS/RESULTS

Analysis The Conversion of Epoxidized Products

Table 1 shows the OOC was determined to be in the range of 4.52 – 4.59. The slightly higher value of OOC in molar ratio of 0.05:2.2 is because the amount of H_2O_2 has produced more water, which enhanced the formation of perfomic acid in epoxidation reaction between HCOOH and H_2O_2 (Mungroo et al., 2008). Similarly, the yield of RCO was achieved up to 97.61% for molar ratio 0.05:2.2, and the higher degree of conversion oxirane was attributed to less steric hindrance and easy availability of epoxy groups to form epoxidized methyl ester (Sahoo et al., 2019).

Table 1 Properties of EWCO-ME at different molar ratio

Ratio HCOOH: H_2O_2	Oxirane Oxygen Content (OOC)	Relative Conversion Oxirane (RCO)
0.05:2.2	4.59	97.61 %
0.6:1.7	4.52	89.94 %

Mechanical Properties of PVC Films

Fig. 1 illustrate the elongation at break (EB) of PVC-40 ratio 0.05:2.2 was the highest at 142.895 %, it is beacause addition plasticizer has enhanced the characteristic of PVC films to be more flexible due to the tendency of opening the hydrogen bond and replaces the hydrogen position in the polymer bonds (Dianursanti et al., 2018). Overall, EB for ratio 0.6:1.7 shows better result for PVC-10 until PVC-30 than ratio 0.05:2.2. The tensile strength of PVC films for PVC-10 resulted 19.56 MPa and 21.51 Mpa for 0.05:2.2 and 0.6:1.7 ratio, respectively. The tensile strength (TS) is related to chemical structure, relative molecular mass, branching and crosslinking. On the contrary, the tensile strength of PVC-40 was low because that the epoxy group weakened the interaction force between the PVC chains (Zhang et al., 2019). Meanwhile, the Young Modulus (YM) value was directly proportional to tensile strength.

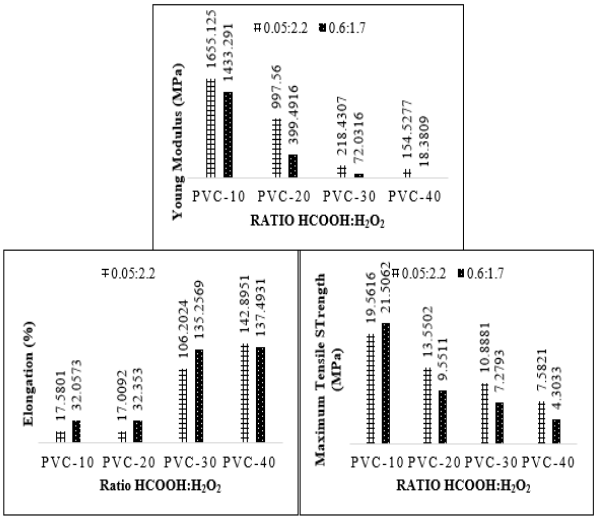

Fig 1 Mechanical properties of PVC-10, PVC-20, PVC-30 and PVC-40 at different epoxidation molar ratio

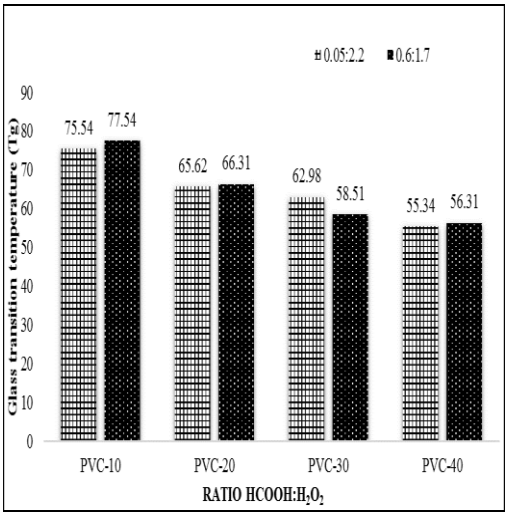

Fig 2 Tg value for PVC-10, PVC-20, PVC-30 and PVC-40 at different epoxidation molar ratio

Glass Transition Temperature of PVC Films

The neat PVC was identify to have Tg value at 96.62 °C. With the increase of plasticizer content, the Tg decreased gradually from 75.54 to 55.34 °C for 0.05:2.2 molar ratio, while the same trend for

0.6:1.7 molar ratio decreased steadily from 77.54 to 56.31 °C as shown in Fig 2. This indicates EWCO-ME can create more free volume in the polymer.

CONCLUSIONS

In conclusion, the waste cooking oil was successfully converted into epoxidized waste cooking oil methyl ester with 0.05:2.2 molar ratio of HCOOH:H_2O_2 reported the highest conversion to 4.59 of OOC value, and RCO at 97.61%. This epoxidation properties result significantly affect the mechanical and thermal properties. PVC-40 was identified as tough and flexible plasticity with EB (142.90 %), TS (7.58 MPa) and YM (154.53 MPa); and Tg value reported dramatically reduce to 55.34°C.

REFERENCES

Chen, J., Liu, Z., Jiang, J., Nie, X., Zhou, Y. & Murray, R. E. (2015) A novel biobased plasticizer of epoxidized cardanol glycidyl ether: synthesis and application in soft poly(vinyl chloride) films. *RSC Advance*, 5, 56171-56180.

Derawi, D., Salimon, J. & Ahmed, W. A. (2014). Preparation of epoxidized palm olein as renewable material by using peroxy acids. *The Malaysian Journal of Analytical Sciences*, 18 (3): 584 – 591.

Dianursati, Gozan M, Windiani L, Sabathini H.A. (2018). Optimizing Characteristic of Spirulina-Polyvinyl Alcohol (PVA) Bioplastic through Protein Deformation with Variation of Heating Time and Solvent's pH. E3S *Web of Conferences*, 67.

Jia, P., Zhang, M., Hu, L., Feng, G., Bo, C. & Zhou, Y. (2015) Synthesis and application of environmental castor oil-based polyol ester plasticizers for poly (vinyl chloride). *ACS Sustain. Chem. Eng*., 3 (9) , 2187-2193.

Kousaalya, A. B., Beyene, S. D., Gopal, V., Ayalew, B. & Pilla, S. (2018). Green epoxy synthesized from *Perilla frutescens*: A study on epoxidation and oxirane cleavage kinetics of high-linolenic oil. *Industrial Crops and Products*. 123, 25-34.

Mungroo R, Pradhan N.C, Goud V.V, Dalai A.K. (2008). Epoxidation of canola oil with hydrogen peroxide catalyzed by acidic ion exchange resin. *Journal of the America oil Chemists' Society*, 85 (9), 887-896.

Sahoo, S. K., Khandelwal, V. & Manik, G. (2019). Synthesis and characterization of low viscous and highly acrylated epoxidized methyl ester based green adhesives derived from linseed oil. *International Journal of Adhesion and Adhesives*. 89, 174-177.

Silva, G. F., Camargo, F. L. & Ferreira, A. L.O. (2011). Application of response surface methodology for optimization of biodiesel production by transesterification of soybean oil with ethanol. *Fuel Processing Technology*. 92, 407-413.

Vaibhav V.G, Narayan C.P, Anand V.P. (2006). Epoxidation of karanja (*Pongamia glabra*) oil by H_2O_2. *Journal America Chemistry Society*, 83(*7*), 635-640.

Yang, Y., Huang, J., Zhang, R. & Zhu, J. (2017) Designing bio-based plasticizers: effect of alkyl chain length on plasticization properties of isosorbide diesters in PVC blends. *Materials & Design*, 126, 29-36

Zhang, H., Zhu, F., Fu, Q., Zhang, X. & Zhu, X. (2019). Mechanical properties of renewable plasticizer based on ricinoleic acid for PVC. *Polymer Testing*. 76, 199-206.

***Keywords*:** waste cooking oil, epoxidation, plasticizer, PVC, films

International Science, Technology and Engineering Conference, (ISTEC 2020) 13-14
e-isbn: 978 -967- 16937-1-1

INVESTIGATION THE EFFECTS OF HNTS AND CNT NANOTUBES REINFORCED PMMA DENTURE BASE ON THE HARDNESS, IMPACT AND FLEXURAL STRENGTH

Issam. M. Aldwimi [1,3], [*]Hazizan. Md. Akil[1,2] and Ahmed. O. Alhareb[3]
[1]*School of Materials and Mineral Resources Engineering, Engineering Campus, Universiti Sains Malaysia, 14300 Nibong Tebal, Palau Penang, Malaysia*
[2]*Cluster of Polymer Composites, Universiti Sains Malaysia, 14300 Nibong Tebal, Penang, Malaysia*
[3]*The Faculty of Medical Technology of Msellata, Almorgab University, Libya*
[*]*hazizan@usm.my*

PURPOSE/AIM & BACKGROUND
Polymethyl methacrylate (PMMA) resin commonly used for the fabrication of denture base that by used heat curing polymerization. The objectives of this work to investigation of the effects the two types of nanotubes technology, halloysite nanotubes (HNTs) and carbon nanotube (CNT) on the impact strength (IS), flexural strength (FS) and Vickers hardness (VH) of PMMA denture base.

METHODOLOGY
The denture base composites were fabricated by incorporating PMMA powder, 0.5wt% of benzoyl peroxide (BPO), fixed nanotubes at 5wt% of HNTs / MWCNTs (5/0, 4.5/0.5, 4/1, 3.5/1.5, and 0/5) nanotubes as powder components. PMMA powder was mixed with a liquid (made from 90% methyl methacrylate (MMA) and10% ethylene glycol dimethyl-acrylate (EGDMA), as a crosslinking agent).

FINDINGS/RESULTS
The results show that the mean of impact strength significantly increased by the incorporation of 5wt% of HNTs/MWCNTs nanotubes with the ratio of (4:1 wt%) by 10.51 KJ/m^{2}compared to unenhanced PMMA. However, the Vicker's hardness of the PMMA decreased by incorporation of 5wt% of HNTs/MWCNTs nanotubes, to 17.42kg/mm^2.

CONCLUSIONS
The addition of HNTs and MWCNTs nanotubes to the PMMA matrix improved the impact strength but not the Vicker's hardness. Therefore, hybrid reinforced PMMA denture base composite with HNT and MWCNT nanotubes fillers is appropriate to be used for high performance prosthodontics applications.

REFERENCES
Abboud M, Vol S, Duguet E. *J Master Sci* 11, 295-300 (2000).
Abdel-Samad A, EL-Fallal A. *Egypt Dent Associat* 55, 639-643 (2009).
Ahmad, Z. Polymer dielectric materials. In. Silaghi, M.A (ed). Dielectric materials. Rijeka, Croatia: In Tech 2012, pp.14 (2012).
Ahmed.O.S. Alhareb. Enhancement of PMMA Denture Base Properties Through Combination of NBR and Ceramic Particles as Fillers. P.hD. Thesis, Universiti Sains Malaysia, (2016).
Alhareb AO, Ahmad ZA. *J Reinf Plast Compos* 30, 83-5 (2011).
Alhareb AO, Akil HBM, Ahmad ZAB. J Thermoplastic Compos Mater 28, 1–22 (2015).
Andrew MB, Pienkowski D. *Copolymer Carbon* 45, 2098-2104(2007).
Archana B, Abhishek B. *J IOH* 6, 121-126 (2014).
Asar NV, Albayrak H, Korkmaz T, Turkyilmaz I. *J. Adv. Prosthodontic* **5**, 241-247 (2013).
Asopa V, Suresh S, Khandelwal M, Sharma V, Asopa S S, Kaira L S. *Saudi J Dent Res* 6, 146 – 151 (2015).
Ayad NM, Badawi MF, Fatah AA. *Rev Clin Pesq Odontol* 4, 145-151 (2008).
Chaijareenont P, Takahashi H. *Dental Materials J* 31, 623-8 (2012).

G. Zappini, A. Kammann, W. Wachter, *J Prosthet Dent*. 90, 578-585 (2003).
H. Akin, F. Tugut, U. Guney, and T. Akar. *Journal of Prosthodontics* 23, 152–156 (2014).
Joussein E, Petit S, Churchman J. *Clay Minerals* 40, 383-426 (2005).
M. M. Gad, A. Rahoma, and A. M. Al, Obity. *Dental Materials Journal* 37, 746– 753 (2018).
Puri G, Berzins DW, Dhuru VB, Raj A, Rambhia SK, Dhir G, Dentino AR. *J Prost Dent* **100**, 302-308 (2008).
Vergaro V, Abdullayev E, Lvov YM, Zeitoun A, Cingolani R, Rinaldi R, Leporatti S. *Biomacromolecules* 11, 820-826 (2010).
Wang R, BillTu JT. *J P D* 3, 318-26 (2014).
Y. Ye, H. Chen, J. Wu and L. Ye. *J Polymer* 48, 6426-6433 (2007).

Keywords: PMMA, Carbon nanotubes , Halloysite nanotubes, Impact strength.

International Science, Technology and Engineering Conference, (ISTEC 2020) 15-17
e-isbn: 978 -967- 16937-1-1

NUMERICAL SIMULATION ANALYSIS OF KENAF REINFORCED POLYPROPYLENE COMPOSITES

*Nabilah Afiqah Mohd Radzuan, Mohammad Afiq Rashid, Dulina Tholibo, Abu Bakar Sulong, Che Hassan Che Haron[5]

[1]*Precision Research Group, Department of Mechanical and Manufacturing Engineering, Faculty of Engineering and Built Environment, Universiti Kebangsaan Malaysia, 43600 Bangi, Selangor, Malaysia,*

*afiqah@ukm.edu.my

PURPOSE/AIM & BACKGROUND

The simulation and modelling method plays an important role in the engineering sector as it aids in determining the effect of factor on the process, functioning as an important engineering tool. Research shows that simulations and modelling serve as a problem solver in predicting the manufacturing parameters which include material forming, pressure and temperature analysis (Choudhury, Lai, & Wong, 2006; Thomas, Oenoki, & Altan, 2000). Studies indicate that the design process is costly at 5 % to 15 % of the total production cost and it is this cost which can be removed by using the modelling and simulation method (Thomas et al., 2000). This method provides significant advantages due to the ability to produce the "virtual" design while conducting the simulation process conducted to ensure that the output is suitable and meet the product specifications. Moreover, this method assists in reducing product defects such as tearing and wrinkling which improve the composite materials and structural analysis (Pickett, 2004). Therefore, natural kenaf fibre is a promising material for future development as it user and environment friendly, recyclable and lightweight (Masoodi, Pillai, Grahl, & Tan, 2012; Tholibon et al., 2016). In this research, PAM-FORM 2G software was used to investigate the processing parameters of kenaf fibre reinforced polypropylene composite at different process parameters including puncher velocity, puncher radius and heating temperature. This paper aims to establish the effect of modelling and simulations used on the materials thickness distributions, strain values and shear angles.

METHODOLOGY

Geometry design

The CATIA V5 software was used to design the geometry models to develop each component including the puncher, lower blank holder and the upper blank holder. The specification of each component was designed according to the hot-pressing technique using a Zwick Sheet Forming machine. The isometric view of the puncher and blank holder components. The puncher was designed at 38 mm x 38 mm square with 50 mm high. The lower blank holder and upper blank holder share the same design dimension with 80 mm x 80 mm x 2 mm height.

Simulation procedure

The previously developed geometry model was imported into the PAM-FORM 2G using the .igs format before correcting the element orientation. Later, the 'ply composite' was developed and the composite material specification such as young modulus, poison ratio and density were inserted. The composite material thickness which is 2 mm was assigned and the 0.5 mesh was recorded. Each component was defined as 'surface tool'. The progression time to control the simulation process was defined as 10 ms.

RESULTS AND DISCUSSION

The thickness distribution of the composite materials is crucial as it ensures that the end product reache an appropriate thickness and distribution (Behrning, Bley, & Joergens, 2001). Other studies reported that contact friction and puncher speed affect the product thickness, as low contact friction causes slippage during the formation process which results in an excellent thickness distribution. However, when composite materials are exposed to higher contact friction between the puncher and the composite layer, the results is an uneven thickness distribution (Hao, Zhao, & Chen, 2013). Figure 1 shows the graphical image of the simulated puncher when applied onto the composite layer where the edge section of the composite layer tends to deform into a curve. Thus, results show that the thickness distribution was excellent on the flat surface while, the decrease in composite layer thickness occurred in the curved areas consequently causing wear and tear. Other studies reported an identical outcome which indicated that the puncher speed plays an important role in maintaining the thickness distributions (Sala, Cassago, & Di Landro, 2002). The interaction between the thickness distributions and the strain value has also been discussed and reported by other studies which explained that the strain value corresponds to the thickness of the composite layer (Zheng, 2012).

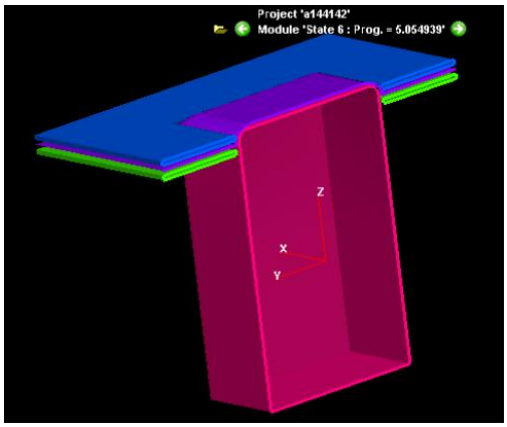

Figure 1: Simulation image of puncher operation onto the composite layer.

CONCLUSIONS

Analysis perform using the kenaf fibre reinforced polypropylene composite material was identially optimised via Taguchi method by considering the puncher speed, puncher radius and heating temperature as the hot-pressing process parameters. Based on the findings, the optimised parameters obtained were recorded at 30 m/s of puncher speed and 2 mm of puncher radius. Meanwhile, the optimum heating temperature recorded at 160 ºC which resulted in maximum thickness distribution of 14.09 mm wothe the shear angle of 2.21º. Upon the three major parameter consider in this study, the puncher speed is the most significant processing parameter which has the ability to minimise the defects occurance, i.e: tearing and wrinkling.

REFERENCES

Behrning, S., Bley, H., & Joergens, S. (2001). Numerical simulations in optimisation of product and forming process. *Journal of Materials Processing Technology*, 115(1), 122–126. Retrieved from https://doi.org/10.1016/S0924-0136(01)00744-0

Choudhury, I. A., Lai, O. H., & Wong, L. T. (2006). PAM-STAMP in the simulation of stamping process of an automotive component. *Simulation Modelling Practice and Theory*, 14(1), 71–81. Retrieved from https://doi.org/10.1016/j.simpat.2005.04.002

Hao, A., Zhao, H., & Chen, J. Y. (2013). Kenaf/polypropylene nonwoven composites: The influence of manufacturing conditions on mechanical, thermal, and acoustical performance. *Composites Part B: Engineering*, 54(1), 44–51. Retrieved from https://doi.org/10.1016/j.compositesb.2013.04.065

Masoodi, R., Pillai, K. M., Grahl, N., & Tan, H. (2012). Numerical simulation of LCM mold-filling

during the manufacture of natural fiber composites. *Journal of Reinforced Plastics and Composites*, 31(6), 363–378. Retrieved from https://doi.org/10.1177/0731684412438629

Pickett, A. K. (2004). *Numerical Simulation As a Tool for Manufacturing, Failure and Impact Prediction of Textile Reinforced Composites*. *Advanced Polymer Composites for Structural Applications in Construction*. Woodhead Publishing Limited. Retrieved from https://doi.org/10.1533/9781845690649.5.535

Sala, G., Cassago, D., & Di Landro, L. (2002). A numerical and experimental approach to optimise sheet stamping technologies: Polymers thermoforming. *Materials and Design*, 23(1), 21–39. Retrieved from https://doi.org/10.1016/S0261-3069(01)00037-1

Tholibon, D., Sulong, A. B., Muhammad, N., Ismail, N. F., Tharazi, I., & Md Radzi, M. K. F. (2016). Tensile properties of unidirectional kenaf fiber polypropylene composite. *Jurnal Teknologi*, 78(6–9), 101–106. Retrieved from https://doi.org/10.11113/jt.v78.9153

Thomas, W., Oenoki, T., & Altan, T. (2000). Process simulation in stamping – recent applications for product and process design. *Journal of Materials Processing Technology*, 98(2), 232–243. Retrieved from https://doi.org/10.1016/S0924-0136(99)00204-6

Zheng, Y. (2012). The Coupled Effects of Thickness and Distance between Holes on Stress and Strain Concentrations of Uniaxially Loaded Tensile Plates. *Applied Mechanics and Materials*, 268–270, 761–766. Retrieved from https://doi.org/10.4028/www.scientific.net/AMM.268-270.761

***Keywords*:** Kenaf fibre, PAM-FORM 2G, hot-pressing.

International Science, Technology and Engineering Conference, (ISTEC 2020) 18-20
e-isbn: 978 -967- 16937-1-1

PERFORMANCE EVALUATION OF CLAM SHELLS AND COCKLE SHELLS AS SOURCE OF CALCIUM-BASED ADSORBENTS IN CARBON DIOXIDE ADSORPTION

Sei Ling Tan[1], *Zhi Hua Lee[2,], Shee Keat Mah[2], Abdul Rahman Mohamed[1]
[1] School of Chemical Engineering, Universiti Sains Malaysia (Engineering Campus), 14300 Nibong Tebal, Pulau Pinang, Malaysia.
[2] Department of Chemical Engineering, Lee Kong Chian Faculty of Engineering and Science, Universiti Tunku Abdul Rahman (Sungai Long Campus), Bandar Sungai Long, Cheras, 43000 Kajang, Selangor Darul Ehsan, Malaysia.
*leezh@utar.edu.my

PURPOSE/AIM & BACKGROUND

Calcium oxide (CaO) has been the most promising carbon dioxide (CO_2) solid adsorbent as it is cheap, widely available, with accessible and noticeable performance. Biogenesis calcium waste enriched with $CaCO_3$ can be one of the sources of CaO. Utilization of these natural wastes as the source of calcium-based adsorbents has been seized for its benefits in production cost reduction and waste minimization. In this study, natural clam (*meretrix meretrix*) shells and cockle (*anadara granosa*) shells were used as the natural calcium source of CaO-derived adsorbents and investigated for their performance in CO_2 adsorption. The approximated retail value of cockle was more than 32 million US Dollars in Malaysia (Boey, Maniam, Hamid, & Ali, 2011). In addition, the composition of $CaCO_3$ in cockle shells is 95 - 99 wt% (Olivia, Mifshella, & Darmayanti, 2015). In the meantime, clam species can be widely found in Malaysian coasts. $CaCO_3$ composition found in natural clams in Malaysia is 98.7 wt% (Zakaria, Zakaria, & Kasim, 2004). The recorded CO_2 adsorption capacities of these CaO-based adsorbents derived from natural clam shells and cockle shells were 7.95 mmol CO_2 / g adsorbent and 9.61 mmol CO_2 / g adsorbent, respectively. The result observed showed there was still a room of improvement for the performance to the ideal theoretical adsorption capacity, 17.86 mmol CO_2 / g adsorbent. The CaO-based adsorbents were then modified for their properties via ethanol-water hydration treatment. It was observed from XRD results that the crystallite size of CaO-derived adsorbents decreased with the increasing of ethanol concentration used in the treatment. Ethanol-hydration treated CaO-based adsorbents were found to achieve higher CO_2 adsorption capacities at 13.67 mmol CO_2 / g adsorbent for natural clam shells-derived CaO and 16.57 mmol CO_2 / g adsorbent for cockle shells-derived CaO. Ethanol was found to play a role in suppressing the growth of CaO crystallites, contributed to higher surface area in achieving higher CO_2 adsorption capacities.

METHODOLOGY

Adsorbent preparation

Natural clam (*meretrix meretrix*) shells and cockle (*anadara granosa*) shells were collected from the local market. The shells were cleaned with water and dried under the sun for few days. The dried shells were then calcined at 900 °C for 4 h. The derived-CaO after calcination were grounded into powder.

Ethanol-hydration treatment

The derived-CaO adsorbents were soaked in ethanol solution for 2 h. The samples were then dried at 100 °C for 5 h in an oven. 2 different ethanol concentrations, 30 % and 50 % were tested for in ethanol hydration treatment.

CO_2 adsorption activity

Thermogravimetric analyzer (TGA) (TA Instruments, SQ100, New Castle, DE, United States) was used to evaluate CO_2 capture performance of the adsorbent samples. A pretreatment was first carried out at 900 °C for 10 min under 100 ml/min N_2 before the commencement of CO_2 adsorption. Next,

CO_2 adsorption study was carried out at 650 °C for 60 min under 100 min/min pure CO_2 flow. In this study, CO_2 adsorption capacity was calculated and expressed in mmol CO_2/g adsorbent.

FINDINGS/RESULTS

Crystallite sizes of the ethanol-hydration treated adsorbents derived from clam shells and cockle shells are tabulated as below. Increase of ethanol concentration in ethanol-hydration treatment has been found to reduce the crystallite size of the adsorbents. This is due to ethanol could affect the nucleation and growth of the crystallite relatively. When the ethanol concentration was higher, more ethanol molecules shielded the surfaces of the crystallites and inhibited the growth of crystallite (Liu, Lu, Feng, & Tang, 2011).

Table: Crystallite sizes of CaO-based adsorbents derived from clam shells and cockle shells and treated with different ethanol concentrations *via* ethanol-water hydration treatment.

Ethanol Concentration (%)	**Crystallite Size (nm)**	
	Clam	**Cockle**
0	88.97	87.53
30	66.88	65.25
50	53.78	42.22

CO_2 capture capacities of CaO-based adsorbents in this study is presented in figure below. It is noticeable that CaO-based adsorbents derived from cockle shells achieved higher CO_2 capture capacity than CaO-based adsorbents derived from clam shells. As the CO_2 capture capacity was significantly affected by the surface area and pore volume of the adsorbents, the treated adsorbents samples which expected to have a higher surface area were observed to have higher CO_2 capture capacities. Ethanol had played a role in enhancing the hydration of the adsorbents as well as maintaining their reactivity in capturing CO_2 (Li, et al., 2008).

The theoretical CO_2 capture capacity of CaO is 17.86 mmol CO_2/g CaO, with equimolar of CaO and CO_2 were reacted via carbonation. As observed from the result, untreated CaO-based adsorbents derived from clam shells and cockle shells were 7.95 mmol CO_2/g CaO and 9.61 mmol CO_2/g CaO, respectively, which were only about half of the theoretical value. Ethanol-hydration treated adsorbents at 30% of ethanol were tested for their CO_2 adsorption performance. It was observed that both of these treated adsorbents have a higher adsorption capacities as shown in figure below. This has clearly showed that ethanol-hydration treatment will be a promising way to improve the properties and hence the CO_2 capture performance of CaO-based adsorbents by altering the strutural properties of the CaO-based adsorbents.

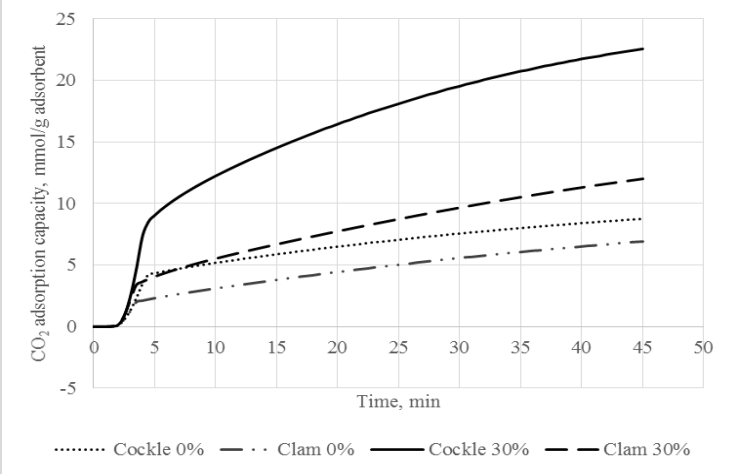

Figure1: CO_2 capture capacities of untreated and treated CaO-based adsorbents derived from clam shells and cockle shells.

CONCLUSIONS

This study has proven that natural clam (*meretrix meretrix*) shells and cockle (*anadara granosa*) can be potential natural sources of calcium-based adsorbent in CO_2 adsorption due to their high $CaCO_3$

composition. The CaO-based adsorbents can be derived from the shells *via* simple calcination process. Ethanol-hydration treatment has found to be helpful in stretching the pore structure of the adsorbents, contributed to higher surface area and pore volume. Crystallite sizes of the adsorbent samples were observed to decrease with the increasing of ethanol concentration used in treatment. In the meantime, CO_2 adsorption capacities were found to increase with the reduction of crystallite size. In conjunction with that, CO_2 adsorption capacities of the adsorbents were improved with ethanol-hydration treatment.

REFERENCES

Boey, P., Maniam, G., Hamid, S., & Ali, D. (2011). Utilization of waste cockle shell (Anadara granosa) in biodiesel production from palm olein: Optimization using response surface methodology. Fuel, 90(7), 2353-2358. doi: 10.1016/j.fuel.2011.03.002

Li, Y., Zhao, C., Qu, C., Duan, L., Li, Q., & Liang, C. (2008). CO_2 Capture Using CaO Modified with Ethanol/Water Solution during Cyclic Calcination/Carbonation. *Chemical Engineering & Technology, 31*(2), 237-244. doi:10.1002/ceat.200700371

Liu, S., Lu, J., Feng, Q., & Tang, W. (2011). Effect of Ethanol on Synthesis and Electrochemical Property of Mesoporous Al-doped Titanium Dioxide via Solid-state Reaction. *Chinese Journal of Chemical Engineering, 19*(4), 674-681. doi:10.1016/s1004-9541(11)60040-2

Olivia, M., Mifshella, A., & Darmayanti, L. (2015). Mechanical Properties of Seashell Concrete. Procedia Engineering, 125, 760-764. doi: 10.1016/j.proeng.2015.11.127

Zuki Abu Bakar Zakaria, Norazri Zakaria and Zaleha Kasim. (2004). Mineral Composition of the Cockle (*Anadara granosa*) Shells, Hard Clamp (*Meretrix meretrix*) Shells and Corals (*Porites spp*.): A Comparative Study . Journal of Animal and Veterinary Advances, 3: 445-447.

Keywords**:** *Clam shells, cockle shells, ethanol-water hydration, calcium-based, CO_2 adsorption*

International Science, Technology and Engineering Conference, (ISTEC 2020) 21-23
e-isbn: 978 -967- 16937-1-1

PHYSICAL AND THERMAL PROPERTIES OF LOW ENERGY CONSUMPTION FIRED INDUSTRIAL WASTE-CLAY BRICKS FROM COCKLE SHELLS AND SODA LIME SILICA GLASS

Rabiatul Adawiyah Abdul Wahab[1, 2], *Maryam Mohammad[1], Mazlini Mazlan[1], Mohammad Aminudin Bin Mohd Razali[1], Nur Arina Binti Mat Rusni[1], W Aisya Nabila Binti W Sharisun Asma[1], Faradihah bt Ashari[1] and Mohd Hafiz Mohd Zaid[2]

[1] *Faculty of Applied Sciences, Universiti Teknologi MARA, Perak Branch Tapah Campus, 35400 Tapah Road, Perak, Malaysia.*

[2] *Department of Physics, Faculty of Science, Universiti Putra Malaysia, 43400 UPM Serdang, Selangor, Malaysia.*

*maryam6328@uitm.edu.my

PURPOSE/AIM & BACKGROUND

Fired clay bricks (FCB) are basic building blocks that had been used since ancient age (Cultrone et al., 2005). The continuously rising demand of FCB in the market increases the use of clay soil which is a non-renewable resource. Due to this, research had been done on using waste materials as clay soil substitution. The use of waste materials not only help economically and environmentally, it also helps to reduce the cost of disposal in landfill sites and to maintain a sound environment (Monteiro et al., 2014). Few of the waste materials used were oyster shell ash (OS) (GengyingLi et al., 2015) and glass waste (Souaibou et. al., 2019). It is found that the application of OS has a positive effect on the increase in strength and durability of bricks in both dry and wet environments. The use of glass as well significantly increase the physical and chemical properties of FCB from industrial waste (Phonphuak et el.) Our study would be on the production of FCB using Malaysia's most common waste which are cockle shells and soda lime silica glass. Mixtures of SLS glass, clay soil and CS were made, and the moulded mixtures are then subjected to firing process. They are characterized for linear shrinkage, bulk density, temperature changes and mechanical strength.

METHODOLOGY

Cockle shells (CS) and soda lime silica glass (SLS) were acquired from Jabatan Nelayan Malaysia and Jabatan Kraf Malaysia respectively. Thereafter, they underwent drying process then grounded and sieved into submicron particle. The admixture of the clay soil, SLS and CS is using empirical formula of $[(CL)_{0.5}(SLS)_{0.5}]_{1-X}[CS]_X$ where X: 0, 0.05, 0.1 and 0.15. Only percentage of 5% and 10% of cockle shell were used due to it being the best composition to be compared with the conventional clay brick and clay brick with SLS. The FCB mixture was fired in the electrical furnace at optimum temperature of 900 °C for 5 hours at the rate of 10 °C/min to form fired clay bricks then subjected to analyses of physical properties by means of linear shrinkage, bulk density, mechanical strength and thermal properties by temperature changes.

FINDINGS/RESULTS

Linear Shrinkage

Figure 1 shows the linear shrinkage percentage of each samples of FCB. The addition of SLS and CS content shows a reduce percentage of linear shrinkage specifically the 10% composition of CS which results in the least shrinking of FCB with 1.98% as compared to conventional FCB from clay with the highest percentage of linear shrinkage with 7%.

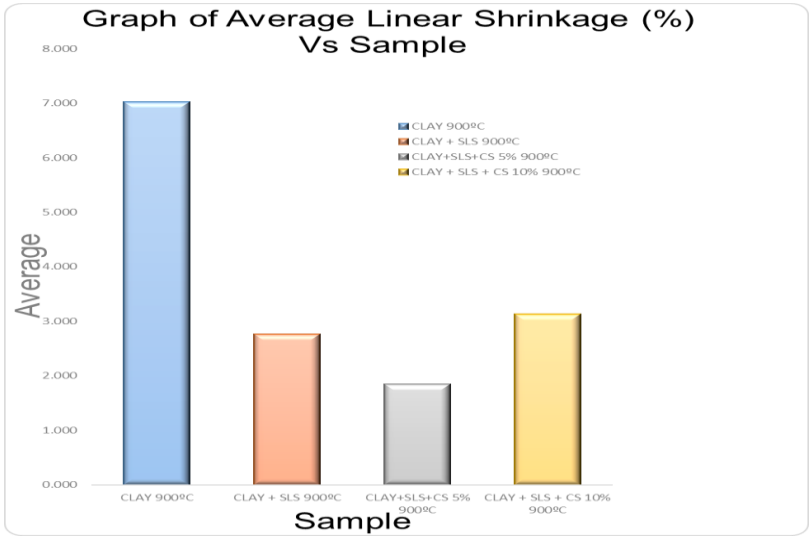

Figure 1: The linear shrinkage of FCB at 900 °C.

Bulk Density

The bulk densities of the specimens are given as below in Figure 2. Comparing between specimen with added SLS + 10% CS and added SLS + 5% CS, the brick specimen with added SLS + 10% CS has bulk density less than with added SLS + 5% CS. The bulk density were highest at 0.0018 g/cm^3 for conventional FCB and decreases the most until 0.0014 g/cm^3 when the CS addition is increased to 10%.

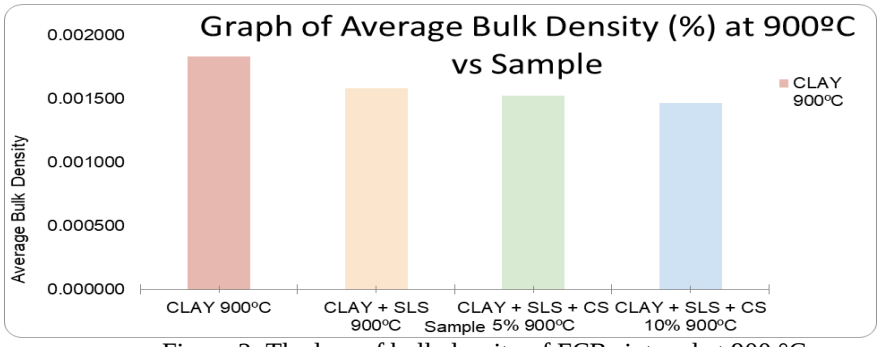

Figure 2: The loss of bulk density of FCB sintered at 900 °C.

Mechanical Strength

Mechanical strength of each sample were calculated and by referring to Table 1, sample of clay + sls + 10% CS showed the highest mechanical strength of 0.54735 N/mm^2 as compared to other samples.

Table 1: Mechanical strength of FCB sintered at 900 °C.

SAMPLE	FORCE (N)	SURFACE AREA (mm^2)	MECHANICAL STRENGTH (N/mm^2)
CLAY (900ºC)	0	1532.1064	0
CLAY + SLS (900ºC)	400	1644.9725	0.24317
CLAY + SLS + CS 5% (900ºC)	200	1639.0927	0.12202
CLAY + SLS + CS 10% (900ºC)	900	1644.2845	0.54735

Heat Conductivity

Results in Figure 3 showed that the sample with addition of SLS and 10% CS has the lowest heat conduction rate of 3200 W proving that it has the highest heat insulation which is required in building materials so that the buildings built are protected from heat and sun effectively.

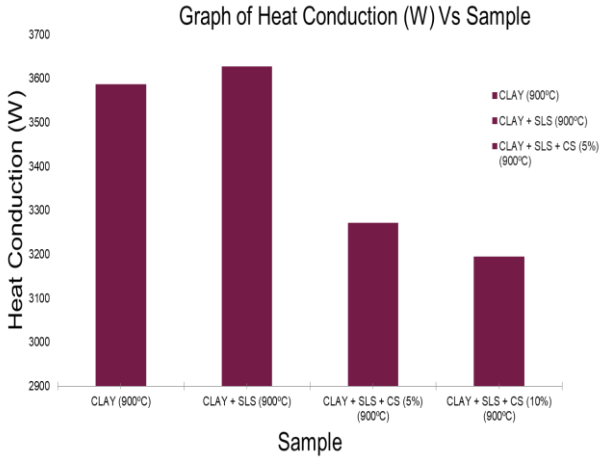

Figure 3: Heat conductivity of FCB sintered at 900 °C.

CONCLUSIONS

It can be concluded that Fired Industrial Waste Clay Brick (FIWCB) from cockle shells and soda lime silica glass was successfully produced with increase in physical and thermal properties at optimum firing temperature of 900ºC and composition of clay soil + SLS + 10% CS. The linear shrinkage decreases and loss of bulk density (BD) decreases as well as highest mechanical strength as compared to other samples. FIWCB from SLS and 10% CS also showed the lowest heat conduction with high thermal insulation.

REFERENCES

GengyingLi, Xiaoyang Xu, E.Chen, Jie Fan, Guangjing Xiong (2015), Properties of cement-based bricks with oyster-shells ash. *Journal of Cleaner Production*, *91*, 279–287.

G. Cultrone, E. Sebastián, M.J. Torre de la (2005). Mineralogical and physical behavior of solid bricks with additives. *Construction and Building Materials*, 19, 39-48.

Monteiro Carlos, Maurício Fontes, On the production of fired clay bricks from waste materials: A critical update. *Construction and Building Materials*, 68, 599-610.

P.L. Boey, G.P. Maniam, S. Abd Hamid and D.M.H. Ali (2011). Utilization of waste cockle shell (Anadara granosa) in biodiesel production from palm olein: Optimization using response surface methodology. *Fuel*, 90, 2353–2358.

Souaibou, Antoine, E., & Raidandi, D. (2019). Influence of the Colorless Waste Glass on the Mineralogical, Microstructural and Mechanical Properties of Clay Material from Wack (Adamawa, Cameroon). *Advances in Materials Physics and Chemistry*, *09*(05), 89–102.

Vorrada Loryuenyong, Thanapan Panyachai, Kanyarat Kaewsimork, Chatnarong Siritai (2009). Effects of recycled glass substitution on the physical and mechanical properties of clay bricks. *Waste Management*, 29(10), 2717-2721.

Yahaya, F. (2019, July 12). Disrupting the brick and mortar industry the green way. *The Malaysian Reserve (TMR) Media Sdn. Bhd.* Retrieved from https://themalaysianreserve.com/2019/07/12/disrupting-the-brick-and-mortar-industry-the-green-way/.

***Keywords*:** Clay soil, cockle shell, bricks, glass.

International Science, Technology and Engineering Conference, (ISTEC 2020) 24-26
e-isbn: 978 -967- 16937-1-1

CURE CHARACTERISTICS AND SWELLING BEHAVIOUR OF NaOH -TREATED PALM KERNEL SHELL (tPKS)/ ACRYLONITRILE RUBBER (NBR) COMPOUNDS

*Noor Aishatun Majid[1], Nor Adabiah Md Nayan[1], Wahida Abdul Rahman[1], Sharifah Nafisah Syed Ismail[1], Noor Faezah Mohd Sani[2], Siti Nur Liyana Mamauod[3], Munirah Onn[4]

[1]*Faculty of Applied Sciences, UiTM Cawangan Perlis, Kampus Arau, 02600 Arau, Perlis*

[2]*Faculty of Applied Sciences, UiTM Cawangan Perak, Kampus Tapah, 35400 Tapah Road, Perak*

[3]*Polymer Composites Research and Technology Center (PoCREST), Institute of Science, Faculty of Applied Sciences, UiTM, 40450 Shah Alam, Selangor*

[4]*Faculty of Applied Sciences, UiTM Cawangan Johor, Kampus Pasir Gudang, 81750 Masai, Johor*

*nooraishatun@uitm.edu.my

PURPOSE/AIM & BACKGROUND

This research used to investigate the effect of NaOH-treated Palm Kernel Shell (tPKS) addition on cure characteristics and swelling behaviour of acrylonitrile butadiene rubber (NBR) compounds using a semi-efficient vulcanization system. It was found that the tPKS slightly increased the scorch time, optimum cure time and crosslink density of the NBR compounds up to 10 phr of loading. From this study, 10 phr of tPKS powder was concluded as an ideal loading in NBR compounds.

METHODOLOGY

Palm kernel shell was dried and ground into the powder size by using pulveriser machine (Chong *et al*., 2017). After that, PKS filler was treated by 6% concentration NaOH for 24 hours. Then, rinsed with water and dried for 24 hours. The PKS/NBR composites were prepared by two roll-mill in accordance to ASTM D 3184 standard. The cure characteristics of rubber compound before processing take place was analyzed accordance to ASTM D-2084. After that, the moulding process was conducted in order to form rubber sheet by using hot press at 160°C.For the crosslink density, the samples were cut with the dimensions of the sample is 10 mm x 10 nnm x 10 mm and dipped in toluene and put in the dark place under room temperature. After 24 hours, the samples were dabbed to remove excess toluene and kept in oven for 70 °C and the dried weight was recorded. The process of drying was repeated until sample weight was constant.

FINDING/RESULTS

Cure characteristics of NaOH-Treated PKS/NBR Composites

Figure 1 shows the scorch time, Ts_2 (min.) and the optimum cure time, Tc_{90} (min.) of uPKS and tPKS filled NBR compounds. It can be observed that by increasing tPKS filled NBR composites will increase the scorch time until optimum loading of 10 phr tPKS is achieved, and then, falls off. It is due to the limitation of the NBR portion and it needs longer time to begin the crosslinking reaction (Daud *et al.*, 2017). Besides, the larger particle size also effects on longer mixing time, hence, it will cause the premature crosslinking (Daud *et al.*, 2017b). Thus, it reduces the Ts_2 and Tc_{90} (min.) of tPKS/NBR compounds lower than uPKS/NBR compounds at 10 phr loading (Ooi *et al*., 2013).

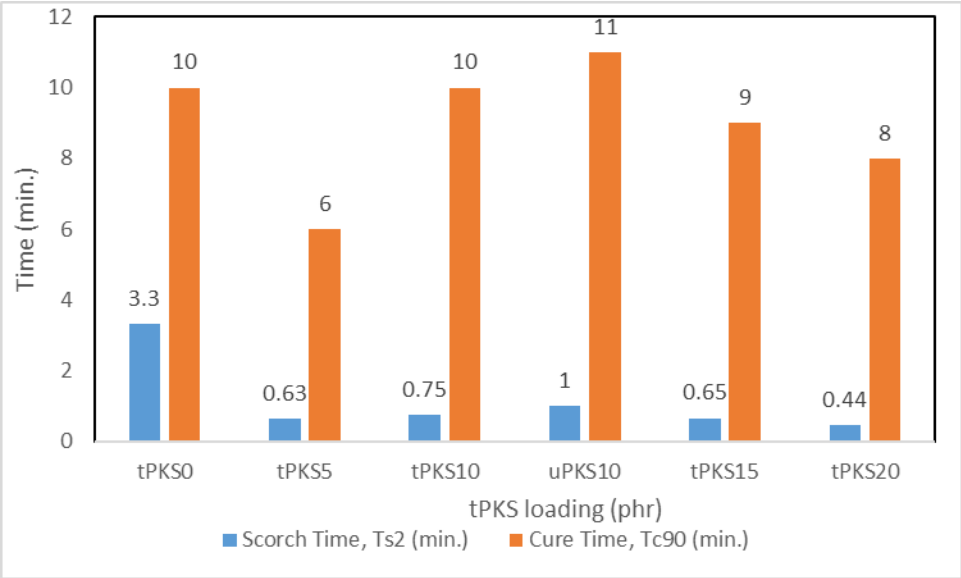

Figure 1: Scorch time & optimum cure time (min.) of the uPKS/NBR and tPKS/NBR Composites

Crosslink Density of NaOH-treated PKS/NBR Composites

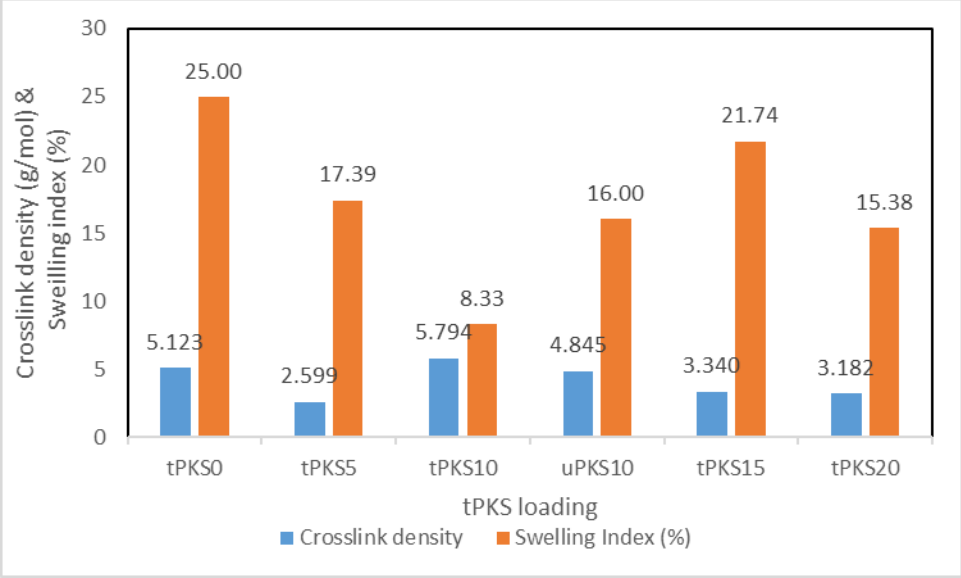

Figure 2: Crosslink Density (g/mol) & swelling index of the uPKS/NBR and tPKS/NBR Composites

Crosslink density of the uPKS/NBR and tPKS/NBR compounds was illustrated in Figure 2. It can be reported that increases trend for the 5 phr to 10 phr of tPKS filled NBR compounds by 55.14 %. It can be seen that tPKS10 shows the highest crosslink density because of 10 phr of tPKS filled NBR compounds is the optimum loading and it contributes to the lowest swelling index. According to Onn *et al.*, (2018), the rubber that has high crosslinking density and hence, less swell due to the better rubber-filler interaction. However, it was drop off when tPKS15 and tPKS20 loading due to the agglomeration of tPKS in NBR matrix. Karthikeyan *et al.*, (2016) also stated that by the increases of the filler loading attributed to the high value of the crosslink density, as it resists the swelling and decreases the uptake of the solvent in cured compounds that lead to better interfacial adhesion.

CONCLUSIONS

In this research, a study on the effect of palm kernel shell (PKS) on cure characteristics and swelling behavior of acrylonitrile rubber (NBR) compounds are presented. Scorch time and cure time was increased until 10 phr loading, then, fall off when tPKS loading increase. Next, as the tPKS loading is increased, crosslink density is also increased.

REFERENCES

Chong, E. W. N., Leong, J. Y., Saurabh, C. K., Dungani, R., Tye, Y. Y., Tahir, P. M., … Abdul Khalil, H. P. S. (2017). Oil Palm Shell Nanofiller in Seaweed-based Composite Film: Mechanical, Physical, and Morphological Properties. *BioResources*, *12*(3), 5996–6010. https://doi.org/10.15376/biores.12.3.5996-6010

Daud, S., Ismail, H., & Abu Bakar, A. (2017a). A Study on the Curing Characteristics, Tensile, Fatigue, and Morphological Properties of Alkali-Treated Palm Kernel Shell-Filled Natural Rubber Composites. *BioResources*, *12*(1), 1273–1287. https://doi.org/10.15376/biores.12.1.1273-1287

Daud, S., Ismail, H., & Abu Bakar, A. (2017b). Soil Burial Study of Palm Kernel Shell-Filled Natural Rubber Composites: The Effect of Filler Loading and Presence of Silane Coupling Agent. *BioResources*, *11*(4), 8686–8702. https://doi.org/10.15376/biores.11.4.8686-8702

Karthikeyan, R., Tjong, J., Nayak, S. K., & Sain, M. M. (2016). Mechanical Properties and Cross-Linking Density of Short Sisal Fiber Reinforced Silicone Composites. *BioResources*, *12*(1), 211–227. https://doi.org/10.15376/biores.12.1.211-227

Onn, M., Mohamad, N. F., Abdul Rani, N. H., & Amir Zulkifly, Z. (2018). Performance evaluation of carbonized rubber seed shell (CRSS) filler as reinforcer in rubber binder. *Malaysian Journal of Fundamental and Applied Sciences, 14*(3), 418–422. https://doi.org/10.11113/mjfas.v14n3.1098

***Keywords*:** Palm kernel shells, acrylonitrile butadiene rubber matrix, cure characteristics, crosslink density, swelling index

International Science, Technology and Engineering Conference, (ISTEC 2020) 27-29
e-isbn: 978 -967- 16937-1-1

BIMETALLIC GOLD-COPPER NANOPARTICLES ON ANODIC ALUMINUM OXIDE (Au-Cu/AAO) MEMBRANE AS A CATALYST FOR REDUCTION OF p-NITROPHENOL

Norizwan Nordin[1,] Hanani Yazid[1,] and Abdul Mutalib Md Jani[2]
[1]*Faculty of Applied Sciences, Universiti Teknologi MARA, 02600 Arau, Perlis, Malaysia*
[2]*Faculty of Applied Sciences, Universiti Teknologi MARA, 35400 Tapah Road, Perak, Malaysia*
*izwan722@gmail.com

PURPOSE/AIM & BACKGROUND

Bimetallic gold-copper nanoparticles (Au-Cu NPs) possess a unique physical and chemical properties which are useful in the application for catalysis (Tursunova et al., 2016). The Au-Cu NPs are often deposited on a support material such as metal oxides, carbon nanotubes (CNTs) or polymers to prevent the aggregation of the nanoparticles (Fang *et al.,* 2017). However, most of the support material is in powder form, making recollection difficult after it has completed its role in the catalytic activity. Hence, one promising approach is the use of nanoporous anodic aluminium oxide (AAO) in the form of a membrane as the support material. AAO has high surface-to-volume ratio, which makes it an excellent choice as a support (Santos et al., 2013). Research by He et al., (2014), finds that Au-Cu NPs showed higher catalytic activity than its monometallic counterpart when reducing *p*-nitrophenol.
Gold-copper nanoparticles (Au-Cu NPs) was successfully synthesized by chemical reduction method followed by grafting the prepared Au-Cu NPs on AAO by spin coating technique. Two formulations of Au-Cu HDA1 and Au-Cu HDA2 were studied in order to produce smaller Au-Cu particle size for further deposition on AAO membrane. Based on UV-Vis results, Au-Cu HDA2 proved to be the best formulation. Meanwhile, vertically aligned and porous structure of AAO membrane was obtained by electrochemical anodization method with 84.17 ± 10.0 nm pore size. This AAO membrane acts as a support for deposition of Au-Cu NPs, which improved the stability as well as prevent the aggregation of Au-Cu NPs. The prepared Au-Cu/AAO was tested as a catalyst for the reduction of *p*-nitrophenol. The highest rate constant (*k*) of 0.0012 s^{-1} was achieved over 10 mg of Au-Cu HDA2/AAO catalyst. The synthesized catalysts were characterized by Fourier Transform Infrared (FTIR) spectroscopy and Field Emission Scanning Electron Microscopy (FESEM) while the catalytic study was monitored using Ultraviolet-Visible (UV-Vis) spectrophotometer.

METHODOLOGY

Synthesis of Au-Cu NPs

About 22.5 mg of hexadecylamine (HDA) and 2 mL of deionized water was added to a vial followed by addition of 0.3 mL of $CuCl_2.2H_2O$ (100 mM), $HAuCl_4.3H_2O$ and 0.28 mL of 1 M glucose solution. The vial was then capped, and the content was magnetically stirred at room temperature for 20 hours. The vial was heated in an oil bath at 100 °C for 3 minutes and then cool by soaking in an ice bath. This formulation was denoted as HDA1. Another Au-Cu formulation was named as HDA2 with the second addition of 15 mg of HDA to the vial and heated for 15 minutes. The vial was then cool in the ice bath.

Fabrication of AAO

The fabrication of AAO was done by two-steps anodization process of aluminium foil (Al). The anodization was carried out using an electrochemical cell. The Al foil was exposed to oxalic acid ($H_2C_2O_4$) under constant voltage of…??? for one minute in an insulated water bath at 5 ° C. The structure form was then immersed in phosphochromic acid solution for 30 minutes before undergoing the second anodization for another 2 hours under the same condition as the first one. Lastly, the Al layer was removed by the CuCl/HCl solution.

Grafting Au-Cu NPs HDA1 and HDA2 on AAO

The synthesized Au-Cu NPs (HDA1 and HDA2) were deposited on the AAO membrane by spin-coating technique. The solution of Au-Cu NPs was spin-coated at 1000 revolutions per minute (rpm) for 60 s respectively. The deposition was repeated three times on the front and back of the membrane without changing the condition. The Au-Cu HDA1/AAO and Au-Cu HDA2/AAO were then dried at 100 ° C for 15 hours in an oven followed by calcination treatment at 400 ° C for 4 hours.

Catalytic Activity

The prepared catalysts were tested for catalytic reduction of *p*-nitrophenol by using UV-Vis spectrophotometer over a scanning range of 200-600 nm. The Au-Cu HDA1/AAO catalyst was put in a cuvette containing freshly prepared $NaBH_4$ and *p*-nitrophenol solution. A decreased in absorbance at 400 nm (λ_{max} *p*-nitrophenolate ion) was observed and rate constant (*k*-value) was calculated. The catalyst that shows the highest catalytic activity will be selected for further study on the effect of catalyst mass.

FINDINGS/RESULTS

Au-Cu HDA2/AAO

After grafting the Au-Cu HDA2 onto the AAO it is found that the average size of the Au-Cu NPs is 220 nm ± 70 nm. Figure 1 shows the FE-SEM image of Au-Cu HDA2/AAO.

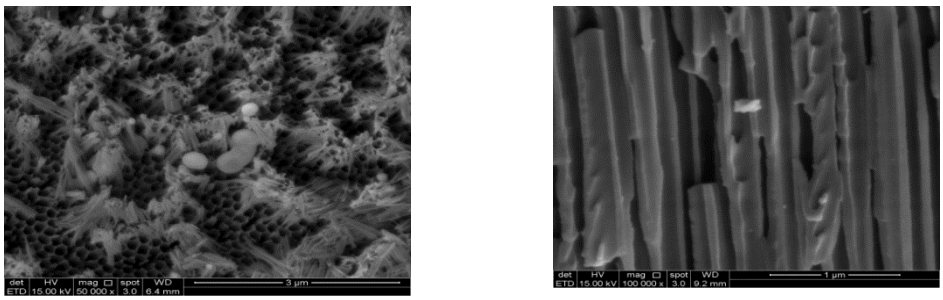

(a) (b)

Figure 1: FE-SEM image of (a) Au-Cu HDA2 attached to the surface AAO membrane and (b) Au-Cu HDA2 attached in the AAO pores (cross section).

Catalytic Reduction of *p*-Nitrophenol

Figure 2 shows a plot of ln A vs time (s) for catalytic reduction of *p*-NP over Au-Cu HDA2/AAO at a various mass of 1 mg, 5 mg and 10 mg. Highest *k*-values of 0.0012 s^{-1} was achieved over 10 mg of Au-Cu HDA2/AAO. The catalytic test was stopped at 10 mg since its already achieved complete reduction with comparable *k*-value as other literature. (Rout et al., 2017) and (He et al., 2014) reported that their Au-Cu NPs have *k*-value of 0.0045s^{-1} and 0.00427s^{-1}, respectively. The summary of *k* values is summarized in Table 1. It can be observed that by increasing the mass of the catalyst, the *k*-value increases.

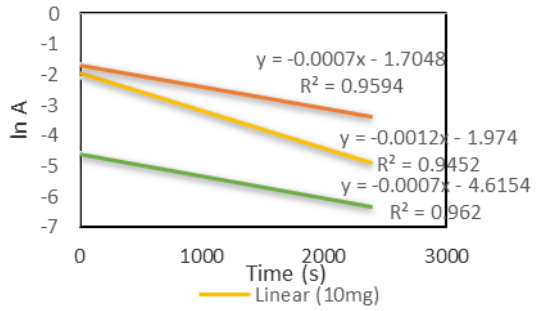

Figure 2: Plot of ln A vs time (s)

Table 1: Mass of catalyst and its *k*-value

Mass of Au-Cu HDA2/AAO **(mg)**	***k*-value (s^{-1})**
1.0	0.0007
5.0	0.0007
10.0	0.0012

CONCLUSIONS

The Au-Cu NPs and AAO were successfully synthesized and fabricated by chemical reduction method and two-steps electrochemical anodization process respectively. The FE-SEM image of Au-Cu HDA2/AAO found that the size of NPs is 220 nm ± 70 nm. In addition, the fabricated AAO have an average pore diameter of 84.17 ± 10.0 nm. The grafting of Au-Cu on AAO prove to be a competitive catalyst with high *k*-value of 0.0012 s^{-1} at 10 mg in the reduction of *p*-np. For instance, extended works are still in progress to further increase the performance of the catalyst.

ACKNOWLEDGEMENT

The authors gratefully acknowledge the support from the Ministry of Higher Education Malaysia for FRGS Grant [600-IRMI/FRGS 5/3 (72/2016)] and Universiti Teknologi MARA, Perlis.

REFERENCES

Ai, L., & Jiang, J. (2013). Bioresource Technology Catalytic Reduction of 4-Nitrophenol by Silver Nanoparticles Stabilized on Environmentally Benign Macroscopic Biopolymer Hydrogel. *Bioresource Technology*, *132*, 374–377.

Chen, H. Y., Wang, J., Ma, P. Y., Liang, J., & Xiang, L. (2015). Influence Of Hydroxylation On Fabrication Of PVC/Caso4composite. *Applied Surface Science*, *357*, 2320–2326.

Fang, W., Deng, Y., Tang, L., Zeng, G., Zhou, Y., & Xie, X. (2017). Synthesis of Pd / Au bimetallic nanoparticle-loaded ultrathin graphitic carbon nitride nanosheets for highly efficient catalytic reduction of *p*-nitrophenol. *Journal of Colloid and Interface Science*, *490*, 834–843.

He, R., Wang, Y.-C., Wang, X., Wang, Z., Liu, G., Zhou, W.,Hou, J. G. (2014). Facile Synthesis Of Pentacle Gold–Copper Alloy Nanocrystals And Their Plasmonic And Catalytic Properties. *Nature Communications*, *5*, 1–10

Rout, L., Kumar, A., Dhaka, R. S., Reddy, G. N., Giri, S., & Dash, P. (2017). Bimetallic Au-Cu Alloy Nanoparticles on Reduced Graphene Oxide Support: Synthesis, Catalytic Activity and Investigation Of Synergistic Effect By DFT Analysis. *Applied Catalysis A: General*, *538*, 107–122.

Santos, A., Kumeria, T., & Losic, D. (2013). Nanoporous Anodic Aluminum Oxide For Chemical Sensing And Biosensors. *TrAC - Trends in Analytical Chemistry*, *44*, 25–38.

Tursunova, R., Yesmurzayeva, N., Selenova, B., & Kudaibergenov, S. (2016). Preparation and Catalytic Activity of Gold–Copper Bimetallic Nanoparticles Stabilized by Poly (N-vinyl-2-pyrrolidone) and Immobilized onto Inorganic Supporters. *Journal of Inorganic and Organometallic Polymers and Materials*, *26*(6), 1259–1263..

Keywords: Au-Cu NPs; AAO; *p*-nitrophenol

International Science, Technology and Engineering Conference, (ISTEC 2020) 30-32
e-isbn: 978 -967- 16937-1-1

ENHANCING AROMATIC HYDROCARBON VIA CATALYTIC PYROLYSIS REACTION ON TORREFIED DEMINERALIZED PALM EMPTY FRUIT BUNCHES (TDPEFB)

*Nur Nasulhah Kasim[1,2], Alina Rahayu Mohamed[3], Mohd Azlan Mohd Ishak[1,2], Razi Ahmad[1,2,4], Khudzir Ismail[1,2]

[1]*Fuel and Biomass Energy Research Group, Universiti Teknologi MARA (UiTM), 40450, Shah Alam, Selangor, Malaysia.*

[2]*Faculty of Applied Sciences, Universiti Teknologi MARA Malaysia (UiTM), 40450 Shah Alam, Selangor, Malaysia.*

[3]*Faculty of Engineering Technology, Unicity Alam, UniMAP, Padang Besar, 02400 Perlis, Malaysia*

[4]*School of Environmental Engineering, Universiti Malaysia Perlis (UniMAP), 02600 Arau, Perlis, Malaysia*.

*nurnasulhah@uitm.edu.my

PURPOSE/AIM & BACKGROUND

Bio-oil derived from biomass through thermal pyrolysis consist of undesirable oxygenated chemical compounds that contribute to low quality of bio-oil. Introduction to catalytic thermal pyrolysis on sequential pre-treatment of biomass shows a promising technique to enhance aromatic hydrocarbon in the bio-oil as an important precursor for the synthesis of additive fuel, pharmaceutical industry and formation of polymeric compounds. Based on previous studies, poor stability, phase separation propensity, high water and acid content, low heating value, and complicated composition of bio-oil come from low grade of raw biomass materials (D. Chen et al., 2017; Stefanidis et al., 2015). In order to produced biomass with low ash and oxygen content, demineralization and torrefaction could eliminate alkali and alkali earth metals (AAEMs) that contribute to ash content and reduce the oxygen content through degradation of hemicellulose, respectively. Further, several aspects of good quality bio-oil such as increased HHV and high-value compounds of bio-oil from pre-treated biomass were monitored and improved (G. B. Chen et al., 2017). Catalytic pyrolysis of biomass over acidic catalysts which is zeolite has attracted significant attention to promote the production of aliphatic and aromatic hydrocarbons through cracking reaction for converting the oxygenated compounds of bio-oil into hydrocarbon under atmospheric pressure (Khanday et al., 2016). Studied by Ro et al., (2018), the bio-oils obtained from the catalytic pyrolysis of palm EFB over the spent FCC and HZSM-5 catalysts produced higher amount of gas and a small amount of bio oil during the catalytic pyrolysis of EFB at 500 °C. Similar finding was reported that HZSM-5 could promote an effective thermal pre-treatment for improving the selectivity of benzene, toluene and xylene (BTX). In this study, the sequential pre-treatments of demineralization and torrefaction palm empty fruit bunches (TDPEFB) followed by catalytic pyrolysis using HZSM-5 was successfully carried out using a fixed-bed reactor in inert nitrogen gas at ambient pressure condition using response surface methodology (RSM). The results from GCMS analysis shows that formation of aromatic hydrocarbon compounds enhanced by 54 % of phenolic and aromatic hydrocarbon compounds in the catalytic thermal pyrolysis of TDPEFB.

METHODOLOGY

Catalytic Thermal Pyrolysis Process

Torrefied demineralized empty fruit bunches (TDPEFB) was carried out using sequential pre-treatment of demineralization and torrefaction based on our previous work. Catalytic thermal pyrolysis experiment was conducted in fixed-bed reactor system. About 5.0 g of PEFB were loaded in a stainless-steel reactor tubing and placed in the fixed-bed reactor for pyrolysis in the inert nitrogen condition. The optimum operation parameters were at 537 (±15 °C) of pyrolysis temperature, 85 °C min^{-1} of heating rate, nitrogen flow rate of 150 mL min^{-1} and holding time for 273 s. The calculation of bio-oil yield, biochar yield and biogas yield were calculated according to Mohamed et al., (2014).

GC-MS Analysis

The chemical compound of bio-oil 1 µL diluted in dichloro methane (DCM) was analysed by gas chromatography-mass spectrometry (GC-MS) model Agilent 6890N equipped with a HP-5MS capillary column (30 m x 250 µm x 0.25 µm nominal). The GC oven temperature was controlled with the programme as follows: (i) 50 °C hold for 3 min, (ii) 50 °C to 180 °C at a rate of 6 °C min^{-1} and (iii) 180 °C to 240 °C rate of 8 °C min^{-1} and held for 30 min. The identification of compound based on computer matching of the peak with the mass of spectra in NIST 08 MS library.

FINDINGS/RESULTS

The Effect of Catalytic Thermal Pyrolysis on Pyrolysis of TDPEFB Product Yields

In an attempt to study the effect of catalytic thermal pyrolysis on the pyrolysis product distribution, Table 1 shows the comparison results for untreated PEFB, TDPEFB and catalytic thermal pyrolysis of TDPEFB at optimized operation condition. Untreated PEFB and TDPEFB were thermal pyrolysed at condition of 490 °C (± 15 °C), pyrolysis temperature, holding time 210 s and at 85 °C min^{-1} of heating rate. Meanwhile, the optimum condition for catalytic thermal pyrolysis were at pyrolysis temperature, holding time, heating rate and catalytic ratio of 537 °C (± 15 °C), 273 s, 85 °C min^{-1} and 10 %, respectively. Beside the sequential pre-treatment, catalytic thermal pyrolysis is another option to increase the percentage of bio-oil yield and enhance the quality of the bio-oil.

Table 1 Pyrolysis products of untreated PEFB, TDPEFB and catalytic PEFB at optimized operation condition

Pyrolysis products	Untreated PEFB (%)	TDPEFB (%)	Catalytic TDPEFB (%)
Bio-oil yield	56.85 ± 0.19	59.53 ± 0.13	59.28 ± 0.23
Biochar yield	22.74 ± 0.21	28.76 ± 0.14	28.78 ± 015
Biogas yield	20.41 ± 0.11	11.71 ± 0.23	11.94 ± 0.37

The attainment of 59.28 % bio-oil yield from catalytic TDPEFB pyrolysis is substantially higher compared to untreated PEFB which about 56.85 %. This finding shows an improvement on thermal pyrolysis of untreated PEFB using fixed-bed reactor system in comparison to previous repeated study on bio-oil yield of 35 % (Mohamed & Hamzah, 2014) and 46.13 % (Azduwin et al., 2015) from untreated PEFB pyrolysis. This result is due to the contribution of initial demineralization step which has successfully removed AAEMs from PEFB since the existence of AAEMs had promoted secondary reactions in biomass pyrolysis that resulted in reduced bio-oil yield (Thangalazhy-Gopakumar et al., 2018). As can be seen, biochar yield follows a similar trend of bio-oil yield which increases from 22.74 % for untreated PEFB to 28.76 % and 28.78 % for thermal pyrolysis of TDPEFB and catalytic thermal pyrolysis of TDPEFB, respectively. However, biogas yield of thermal pyrolysis and catalytic thermal pyrolysis of TDPEFB show in direct contrast compared to bio-oil and biochar yield. This can be explained as increased in coke formation due to insufficient hydrogen capture of active radicals during the reaction of pyrolysis. Interestingly, catalyst play a significant role as cracking agent that invoked the cracking of non-volatile oligomers into monomerics resulting increased in high bio-oil yield.

On the other hand, sequential pre-treatment of TDPEFB shows comparable value of thermal pyrolysis product yields compared to the catalytic thermal pyrolysis of TDPEFB due to the effect of sequential pre-treatments. Remarkably, the optimum HZSM-5 presence of 10 % during the thermal pyrolysis process enhance yield of valuable compounds such as aromatic and phenolic compounds formation (Iliopoulou et al., 2019). The main compounds identified in all three bio-oils can be classified into 7 groups which are ester, hydrocarbon, carbonyl, phenolic compounds, furan, organic acid and nitrogen-containing compounds. From the result shows in Figure 1, bio-oil from catalytic TDPEFB produced aromatic hydrocarbon increased about three times which is 9.35 % compared with bio-oil from non-catalytic of TDPEFB, only 2.19 %. Phenolic compound indicated the similar trend clearly increased to 44.27 % for catalytic TDPEFB pyrolysis. Interestingly, organic acid, carbonyl and furans groups showed the reduction in bio-oil of catalytic TDPEFB pyrolysis. This indicated that during thermal catalytic pyrolysis of TDPEFB, deoxygenation, decarboxylation, decarbonylation and cracking reactions occurred.

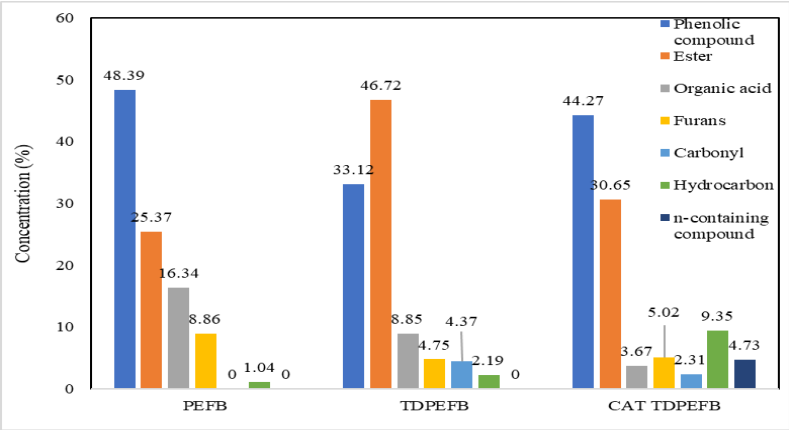

Figure 1: Percentage area of functional group compounds obtained in bio-oil.

CONCLUSIONS

Bio-oil enhance with aromatic hydrocarbon and phenolic compound by 54 % as well as reduced in oxygenated compounds was successfully produced from catalytic thermal pyrolysis of torrefied demineralized palm empty fruit bunch (TDPEFB) in the presence of HZSM-5.

REFERENCES

Azduwin, K. ., Ridzuan, M. J. M. ., Mohamed, A. R. ., & Hafis, S. M. . (2015). Pyrolysis of empty fruit bunch (EFB) in a vertical fixed bed reactor. *Applied Mechanics and Materials*, *695*, 228–231. https://doi.org/10.4028/www.scientific.net/AMM.695.228

Chen, D., Cen, K., Jing, X., Gao, J., Li, C., & Ma, Z. (2017). An approach for upgrading biomass and pyrolysis product quality using a combination of aqueous phase bio-oil washing and torrefaction pretreatment. *Bioresource Technology*, *233*, 150–158. https://doi.org/10.1016/j.biortech.2017.02.120

Chen, G. B., Li, Y. H., Chen, G. L., & Wu, W. T. (2017). Effects of catalysts on pyrolysis of castor meal. *Energy*, *119*, 1–9. https://doi.org/10.1016/j.energy.2016.12.070

Iliopoulou, E. F., Triantafyllidis, K. S., & Lappas, A. A. (2019). *Overview of catalytic upgrading of biomass pyrolysis vapors toward the production of fuels and high-value chemicals*. *November 2017*, 1–29. https://doi.org/10.1002/wene.322

Khanday, W. A., Kabir, G., & Hameed, B. H. (2016). Catalytic pyrolysis of oil palm mesocarp fibre on a zeolite derived from low-cost oil palm ash. *Energy Conversion and Management*, *127*, 265–272. https://doi.org/10.1016/j.enconman.2016.08.093

Mohamed, A. R., & Hamzah, Z. (2014). An alternative approach for the screening of catalytic empty fruit bunch (EFB) pyrolysis using the values of activation energy from a thermogravimetric study. *Reaction Kinetics, Mechanisms and Catalysis*, *114*, 529–545. https://doi.org/10.1007/s11144-014-0798-8

Mohamed, A. R., Hamzah, Z., & Daud, M. Z. M. (2014). Optimization of the pyrolysis process of empty fruit bunch (EFB) in a fixed-bed reactor through a central composite design (CCD). *AIP Conference Proceedings*, *1605*(Ccd), 1172–1177. https://doi.org/10.1063/1.4887756

Ro, D., Kim, Y., Lee, I., Jae, J., Jung, S., Chai, S., & Park, Y. (2018). *Bench scale catalytic fast pyrolysis of empty fruit bunches over low cost catalysts and HZSM-5 using a fi xed bed reactor*. *176*, 298–303.

Stefanidis, S. D., Heracleous, E., Patiaka, D. T., Kalogiannis, K. G., Michailof, C. M., & Lappas, A. A. (2015). Optimization of bio-oil yields by demineralization of low quality biomass. *Biomass and Bioenergy*, *83*, 105–115. https://doi.org/10.1016/j.biombioe.2015.09.004

Thangalazhy-Gopakumar, S., Wei Lee, C., Gan, S., Kiat Ng, H., & Yee Lee, L. (2018). Comparison of Bio-Oil Properties from Non-Catalytic and In-Situ Catalytic Fast Pyrolysis of Palm Empty Fruit Bunch. *Materials Today: Proceedings*, *5*(11), 23456–23465. https://doi.org/10.1016/j.matpr.2018.11.088

***Keywords*:** Catalytic thermal pyrolysis, demineralization, torrefaction, HZSM-5, bio-oil.

International Science, Technology and Engineering Conference, (ISTEC 2020) 33-35
e-isbn: 978 -967- 16937-1-1

$LaSrCoFeO_3$-$Ba(Ce, Zr)O_3$ NANOPARTICLES : SUPERIOR COMPOSITE CATHODE MATERIALS FOR PROTON CONDUCTING FUEL CELL APPLICATION

*Nurul Izzati Abd Malek[1], Ismariza Ismail[2], Abdul Mutalib Md Jani[1,3] and Nafisah Osman[1,4]
[1]*Proton Conducting Fuel Cell Research Group, Faculty of Applied Sciences, Universiti Teknologi MARA, 40450 Shah Alam, Selangor, Malaysia*
[2]*Faculty of Engineering Technology, Universiti Malaysia Perlis, 02100 Padang Besar, Perlis, Malaysia*
[3]*Faculty of Applied Sciences, Universiti Teknologi MARA, 35400 Tapah Road, Tapah, Perak, Malaysia*
[4]*Faculty of Applied Sciences, Universiti Teknologi MARA Perlis, Arau Branch, 02600 Arau, Perlis, Malaysia*
*izzatimalek45@gmail.com

PURPOSE/AIM & BACKGROUND

Proton conducting fuel cell (PCFC) is a green technology system, operates at intermediate temperature between 600 to 800^{o}C that used in portable and mobile devices. A major limitation that inhibits the performance of the overall cell system is a high cathode polarization resistance (R_p) (Ricote et al., 2012). This is due to the lack of surface active site present for oxygen reduction reaction (ORR) that constribute to meeting point between electrolyte, electrode and gas phase which known as triple phase boundary (TPB). Researchers have found several alternatives to improve the TPB length and one of them by introducing composite cathode (Zhou et al., 2013).

LSCF is a well known cathode materials used for PCFCs because it carries both ionic and electronic species that improved from the conventional cathode materials. Recently, addition of some protonic species to the LSCF cathode is believed to lengthen the TPB. The optimum ratio for composite cathode reported was 70:30 for LSCF to BCZY (Osman et al., 2016). In this work, LSCF-BCZY composite cathode is prepared based on the optimum ratio and coated on both sites of the BCZY body that act as a support. The fabricated symmetrical half-cell was then introduced to electrochemical study using an electrochemical impedance spectroscopy (EIS) and morphology of the cell was evaluated using scanning electron microscope (SEM).

METHODOLOGY

LSCF-BCZY composite cathode powder was synthesized via a modified sol-gel method. A stoichiometric amount of La, Sr, Co, Fe (nitrate based salt) was dissolved one-by-one in deionized water, followed by addition of citic acid and ethylenediaminetetraacetic acid (EDTA). The solution was then adjusted to alkaline condition (pH9) using ammonium hydroxide solution and followed by addition of ethylene glycol. The heating treatment of the gel was conducted at 900^{o}C for 5 hours and the black solid was labelled as LSCF. The preparation of the BCZY powder was carried out as previously reported (Abdullah, Hasan, & Osman, 2013). In this study, the composition of 70 : 30 weight percent (wt%) of LSCF to BCZY was formulated. The LSCF-BCZY composite was then transformed into cathode slurry using 6% ethyl cellulose and terpeniol binder, followed by sonicating and stirring methods. The slurry was coated under optimize condition (2000 rpm for 30 seconds) onto BCZY pellet. The symmetrical half-cell of LSCF-BCZY|BCZY|LSCF-BCZY was sintered at 900^{o}C for 1 hour and subjected to electrochemical study using electrochemical impedance spectroscopy (EIS). The EIS spectra was recorded between 1 MHz to 10 mHz using an equivalence circuit of Rs(R1Q1)(R2Q2). The morphological of the cross-sectional cell was observed using scanning electron microscope (SEM) and energy dispersive X-ray (EDX).

FINDINGS/RESULTS

Figure 1 presents the impedance spectrum of LSCF-BCZY|BCZY|LSCF-BCZY at 700^{o}C under wet air atmosphere. The responses was well fitted using equivalent circuit of Rs(R1Q1)(R2Q2). Rs corresponds to ohmic resistance, R1Q1 associated with charge transfer reaction that involved the

transfer of ion from electrolyte to the cathode layer with capacitance value of 3.08×10^{-5} Fcm^{-2} and R2Q2 related to oxygen adsorption or dissociation at the cathode site (capacitance : 2.58×10^{-2} Fcm^{-2}). The ASR value of the composite cathode was 0.45 Ωcm^2. This result was in-line as reported by other work (Lee et al., 2018) as the addition of protonic phase to MIEC electrode has extended the meeting point between electrolyte, electrode and gas phase and promotes more surface active region for high electrochemical reaction. Thus, the preliminary study of electrochemical responses signifies that the composite cathode has shown a good potential for PCFC application.

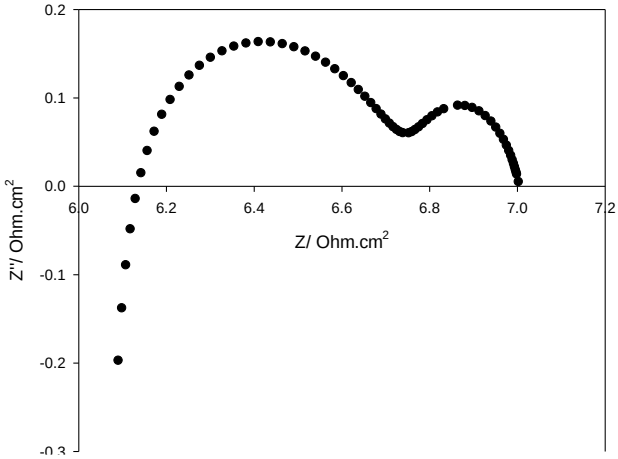

Figure 1. The EIS spectrum of LSCF-BCZY|BCZY|LSCF-BCZY performed at 700ºC under wet air atmosphere

Figure 2 show the morphology of the cross-sectional part of fractured half-cell. The good contact layer was observed between electrode and electrolyte. The thickness of the cathode film was about 8 µm as measured by ImageJ software.

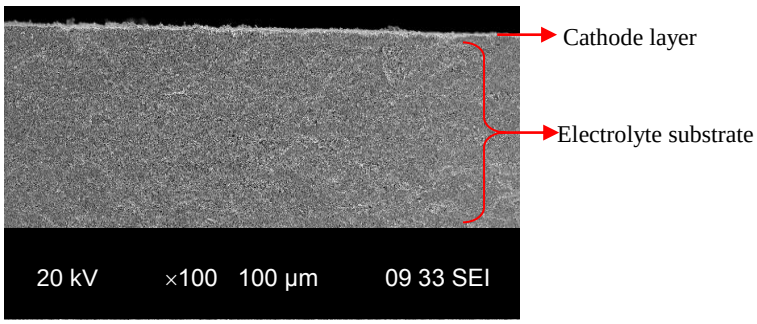

Figure 2. The cross-sectional at image of the half-cell after the EIS analysis

CONCLUSIONS

The modification of the pure cathode material to become composite cathode exhibited the ASR value of 0.45 Ωcm^2 at 700ºC. The enhancement of the cathode was due to the high surface active site that attributed to the increased of TPB length. The good contact layer between electrolyte and cathode layer allow the vast electrochemical reaction in the cell.

ACKNOWLEDGEMENT

We thanks to the Ministry of Education (MOE) Malaysia under Fundamental Research Grant Scheme (ID: 600-IRMI/FRGS 5/3 (2017)) for the support and Universiti Teknologi MARA for the facilities.

REFERENCES

Abdullah, N. A., Hasan, S., & Osman, N. (2013). Role of CA-EDTA on the synthesizing process of cerate-zirconate ceramics electrolyte. *Journal of Chemistry*, *2013*.

Lee, S., Park, S., Wee, S., woo Baek, H., & Shin, D. (2018). One-dimensional structured La0. 6Sr0. 4Co0. 2Fe0. 8O3− δ-BaCe0. 5Zr0. 35Y0. 15O3− δ composite cathode for protonic ceramic fuel

cells. *Solid State Ionics*, *320*, 347–352.
Osman, N., Ismail, I., Samat, A. A., & Md Jani, A. M. (2016). Reactivity study of LaSrCoFeO3 - Ba(Ce,Zr)O3 composite cathode material. *Materials Science Forum*, *846*, 58–62. https://doi.org/10.4028/www.scientific.net/MSF.846.58
Ricote, S., Bonanos, N., Rørvik, P. M., & Haavik, C. (2012). Microstructure and performance of La0. 58Sr0. 4Co0. 2Fe0. 8O3− δ cathodes deposited on BaCe0. 2Zr0. 7Y0. 1O3− δ by infiltration and spray pyrolysis. *Journal of Power Sources*, *209*, 172–179.
Zhou, G. H., Fu, X. Z., Luo, J. L., Chuang, K. T., & Sanger, A. R. (2013). Ag modified LSCF as cathode material for protonic conducting SOFCs. *Materials Technology*, *28*(1–2), 3–8. https://doi.org/10.1179/1753555712Y.0000000035

***Keywords*:** Ultrafine cathode, proton conducting fuel cell, sol-gel, single cell

International Science, Technology and Engineering Conference, (ISTEC 2020) 36-38
e-isbn: 978 -967- 16937-1-1

FISH GELATIN FILM INCORPORATED WITH LEMONGRASS EXTRACT FOR FRUIT WRAPPING APPLICATION

*Salamiah Zakaria,Nur Fathin Hidayah Zamri, Wahida Abdul Rahman and Sharifah Nafisah Syed Ismail
Faculty of Applied Sciences, UiTM Cawangan Perlis, Kampus Arau, 02600 Arau, Perlis,
**salamiah882@uitm.edu.my*

PURPOSE/AIM & BACKGROUND

Currently the world is facing huge problem about the decomposition of synthetic plastic material that used to wrap and to package the foods, fruits and vegetable. Petro-chemical based plastic has been used because it is cheaper, and its mechanical performance is good. However, the usage of synthetic plastics needs to ban and reduce because they are non-recyclable, and non-biodegradable. Hence it will give bad complication and lead to disaster ecological problem.

Protein-based film by from fish has received recognition as a demanding packaging, because of their good performance especially gas barrier, biodegradation and environmental friendly aspect. (Tongnuanchan, Benjakul, and Prodpran, 2014). It has been reported that the addition of active ingredient (essential oil) improved the antioxidant activity of gelatin films. As for the consequences, the packaging material that based on gelatin film is qualify for food protection and preservation. (Tongnuanchan et. al., 2013).

This research is concerned with the development of ecologically clean natural food wraps production using fish waste products. For this study lemongrass extract was used as an active agent and incorporated with gelatin film extracted from Nile tilapia's fish scales. Mechanical properties and physical properties of the incorporated film was determined as well as the quality changes of fruit wrapped with gelatin film incorporated with lemongrass extract.

METHODOLOGY

Lemongrass Extraction

The dried lemongrass was extracted in 200 mL ethanol by using Soxhlet method. The extraction process was performed for a total of at least 6 hours. After the process finished, the ethanol was evaporated using a rotary evaporator, leaving a small yield of extracted lemongrass in the glass bottom flask. The extracted lemongrass was weighed and placed in the sample container and sealed tightly for further used.

Gelatin Extraction

The gelatin from Nile tilapia's fish scales was extracted by using warm distilled water as described by Zakaria and Bakar (2015).

Preparation of Gelatin Film Incorporated with Lemongrass Extract

The incorporated film was prepared by using the method as described by Li et al., (2014) with slight modification.

Characterization of the Films

Antioxidant of the films were evaluated using free radical scavenging activity through diphenylhydrazyl (DPPH) Assay. The functional groups of the control film (gelatin film without lemongrass extract) and the incorporated film were determined by using attenuated total reflectance-Fourier transform infrared spectroscopy (ATR-FTIR). The thickness of the films were measured using Handheld micrometer with 0.001 mm accuracy. The mechanical properties (Tensile strength (TS), elastic modulus (EM) and elongation at break (EAB) of both films were determined by using the Instron Machine equipped with tensile load cell of 100 N. The moisture content and water solubility of both films were also measured. The quality changes of fruits (cherry tomatoes) were determined by wrapping the fruits with the incorporated film as well as the control film at room temperature for 14 days. Within 14 days, the appearances of the fruits were determined in term of the fruits' shrinkage and percent weight loss.

FINDINGS/RESULTS

The calculated percent yield for lemongrass extract was 22.5 %. The percent yield of gelatin extracted from Nile tilapia's fish scale was 16.0 %. The similar percent yield was reported by the previous study done by Zakaria and Bakar (2015) for gelatin extracted from the scales of black tilapia.

From the results of DPPH scavenging activity, it can be concluded that film solution that incorporated with lemongrass extract was able to inhibit free radical due to high amount of inhibition which is 72.50% at concentration of 125 ppm. This might be due to the content of phenolic compound and flavonoid constituent in the film solution. (Ganiari et al., 2017). This finding suggested that film solution incorporated with lemongrass extract is relatively potential has antioxidant agent.

The absorption peaks at 1584.13 cm^{-1}, 3317.68 cm^{-1}, 1478 cm^{-1} and 2852 cm^{-1} for FTIR spectrum of incorporated film confirmed the presence of –N-H, –OH,C = C and C-H groups respectively groups which indicated that incorporated film contain flavonoids and terpenoids (Basera, Lavania, Agnihotri, and Lal, 2019)

It was found that the thickness of the incorporated film was 0.20 mm which is higher than that of the control film (0.15 mm). Lemongrass extract droplets might insert and localize themselves in the film network, which can improve the cross linking between the bond in the film matrix. As for mechanical properties, the incorporated film had highest EAB but lower TS and YM, as compared with the control film. TS of films decreased as the lemongrass extract were added due to protein–protein interaction by the replacement of lipids occurred in film network (Tongnuanchan, Benjakul, and Prodpran, 2014). According to Yang and Paulson (2000), the interactions between non-polar molecules and polymers molecules are much lower than those polar polymer molecules. Plant extract, crude oil contains high amount of non-polar molecules or hydrophobic compounds, such as monoterpene hydrocarbon, which could reduce the compactness of film network as evidenced by the decreased in TS and YM of the film.

The moisture content of control film and incorporated film are 23.12% and 13.17% respectively. The film incorporated with lemongrass extract has low moisture content due to the ability of the lemongrass extract incorporated with gelatin film reduced the water content in the film to enhance the stability of the film. The incorporated film demonstrated slightly higher water solubility than control film. Commonly, high water solubility of incorporated film may indicate the lower water resistance. However, high water solubility may be an advantage for some applications especially in fruit wrapping. The film with high water solubility can be degraded rapidly and modified easily to improve their physical and chemical properties (Li et al., 2014).

The quality changes of cherry tomatoes (unwrapped, wrapped with control film and wrapped with incorporated film) were successfully observed and recorded. All of cherry tomatoes experienced weight loss due to shrinkage of fruit and they get lighter day by day. At day-14, it was found that the unwrapped cherry tomato has highest weight loss (21%) followed by cherry that wrapped with control film (19%) and incorporated film (16%). It is also observed that cherry tomato wrapped with incorporated film shrunk slower than the other two which got shrunk and swollen badly starting from day-7. This proven film incorporated with that lemongrass extract helped in prolonging the shelf-life of fruit at room temperature. This might due to the presence of antioxidant compound from lemongrass extract that slow down the oxidization process of the fruits.

CONCLUSIONS

The incorporation of lemongrass extract to the gelatin film extracted from Nile tilapia's fish scales improved the physical and mechanical properties of the film. The incorporated film also contribute in extending the fruits' shelf life due to the presence of antioxidant compound from lemongrass extract. Therefore, gelatin film incorporated with lemongrass extract show a potential to be used for fruit wrapping application.

REFERENCES

Basera, P., Lavania, M., Agnihotri, A., & Lal, B. (2019). Analytical Investigation of Cymbopogon citratus and Exploiting the Potential of Developed Silver Nanoparticle Against the Dominating Species of Pathogenic Bacteria. 10(February), 1–13.

Ganiari, S., Choulitoudi, E., & Oreopoulou, V. (2017). Edible and active films and coatings as carriers of natural antioxidants for lipid food. *Trends in food science & technology*, *68*, 70-82.

Li, J. H., Miao, J., Wu, J. L., Chen, S. F., & Zhang, Q. Q. (2014). Preparation and characterization of active gelatin-based films incorporated with natural antioxidants. *Food Hydrocolloids*, *37*, 166–173.

Tongnuanchan, P., Benjakul, S., & Prodpran, T. (2013). Physico-chemical properties, morphology and antioxidant activity of film from fish skin gelatin incorporated with root essential oils. *Journal of Food Engineering*, *117*(3), 1571–1579.

Tongnuanchan, P., Benjakul, S., & Prodpran, T. (2014). Comparative studies on properties and antioxidative activity of fish skin gelatin films incorporated with essential oils from various sources. *International Aquatic Research*, *6*(2), 1–12.

Yang L, Paulson AT (2000) Effects of lipids on mechanical and moisture barrier properties of edible gelatin film. *Food Res Int* 33(7):571–578

Zakaria, S., and Bakar, N. H. A. (2015). Extraction and Characterization of Gelatin from Black Tilapia (Oreochromis niloticus) Scales and Bones. International Conference on Advances in Science, Engineering, Technology & Natural Resources (ICASETNR-15) Aug. 27-28, 2015 Kota Kinabalu (Malaysia)

***Keywords*:** gelatin films, lemongrass,fruit wrapping

International Science, Technology and Engineering Conference, (ISTEC 2020) 39-41
e-isbn: 978 -967- 16937-1-1

CHARACTERISATION ON GREEN COATING RESIN OF MALEINATED SOYBEAN OIL

*Sharifah Nafisah Syed Ismail, Mithalina Zulaikha Ismail, Salamiah Zakaria, Noor Aishatun Majid, Nor Mazlina Abdul Wahab and Wahida Abdul Rahman
Universiti Teknologi MARA, Faculty of Applied Sciences, Uinversiti Teknologi MARA, 02600 Arau, Perlis, Malaysia,
*sharifahnafisah@uitm.edu.my

PURPOSE/AIM & BACKGROUND

Bio-based coating can be defined as utilization of organic compounds, recyclable, and non-toxic to the environment. Renewable resources such as vegetable oils, fatty acid and industrial starches can be used as the sources of bio-based coating. Recently, the potential utilization of chemically modified vegetables oils has been paid a high consideration as raw materials to produce modified thermoset polymer (Rucigaj *et al.,* 2014). This is because, they have a specific structure that can be categorized by the existence of dissimilar types of fatty acids in a triglyceride structure (Espana, *et al.,* 2012). This triglycerides groups can undergo reaction such as acylation, isomerization, hydrogenation, hydroxylation, oxidative cleavage, carboxylation and epoxidation. Nevertheless, epoxidized soybean oil (ESO) that has the epoxy group functionality has several weaknesses such as less reactivity and prone to produce intra-molecular bonding that show a tendency to initiate limited thermal and mechanical properties of polymer. Hence, ESO which is made up from epoxidation process of soybean oil can be further modified into maleinated soybean oil (MSO) by incorporating maleic anhydride under esterification process (Li, *et al.,* 2017). MSO has a high potential to be used in the application of bio-based coating. Maleic anhydride act as a hardening agent that make the ESO to toughen along the crosslinking of the chains. The anhydride groups with long chain backbones will contribute to produce good flexural strength to the bio-film product. Thus, the current study intends to enhance the usage of ESO functionalized maleic anhydride for the bio-coating film applications.

METHODOLOGY

Preparation of Maleinated Soybean Oil

The maleinated process was carried out by the mixture of 100g of ESO and 64.7g of maleic anhydride together with 0.10g of hydroquinone and 100g of ethanol. The mixture was heated up to 80-90°C until homogenous solution was formed. Acid value (AV) and oxirane oxygen content (OOC) test were measured at every 30 minutes interval until a near constant acid values was achieved. The OOC and AV test were measured from starting until the reaction was completed.

Oxirane Oxygen Content (OOC) Test

OOC was carried out for the characterization of MSO. It was used to define the amount of oxirane groups produced in place of double bonds by wet titration. The value of OOC for MSO was determined by using ASTM D1652-11.

Acid Value (AV) Test

Acid value test by using the AOCS Cd 3d-63 was used for the characterization of MSO. It is described as the amount of KOH in milligram required to neutralize the organic acids exist in 1 gram of fat. It is also used to measure the amount of the free fatty acids existing in the MSO.

FINDING/RESULTS

Oxirane Oxygen Content (OOC)

The oxirane oxygen content value for the sample was taken every 30 minutes during esterification process. The values of OOC are gradually decreasing with reaction time as can be seen in Figure 1. It indicates a ring opening of epoxide group from ESO that allow ester group from maleic anhydride to form on the backbone of MSO. Lui *et al.,* (2005) study on the synthesis and testing of

soy-based polyols and they stated that the reduction of oxirane oxygen content was due to the oxirane opening polymerization underwent by the polyols. To relate with this study, the reduction of oxirane oxygen content in the sample was caused by the substitution of epoxide group with ester group from the process of esterification.

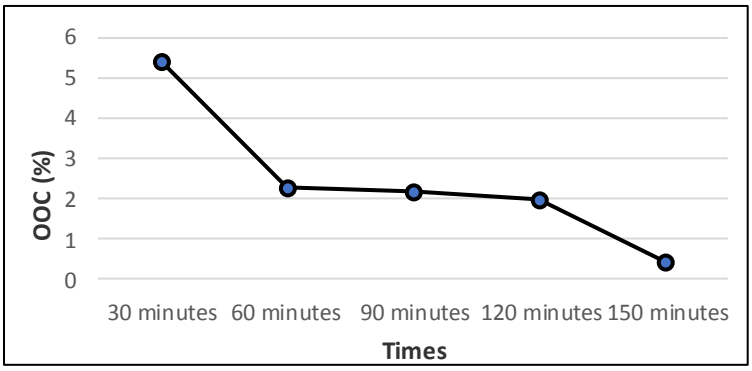

Figure 1: Graph OOC value for MSO sample

Acid Value Test

AV test was done on each sample of MSO by taking 5 gram of the sample every 30 minutes and mixed with the phenolphthalein indicator in the conical flask. The mixture was titrated with potassium hydroxide solution and the changed in color was observed during the titration. The result was shown in Figure 2. Based on the result, the acid value for each sample that was taken every 30 minutes was decreased as the time increased (Figure 2).

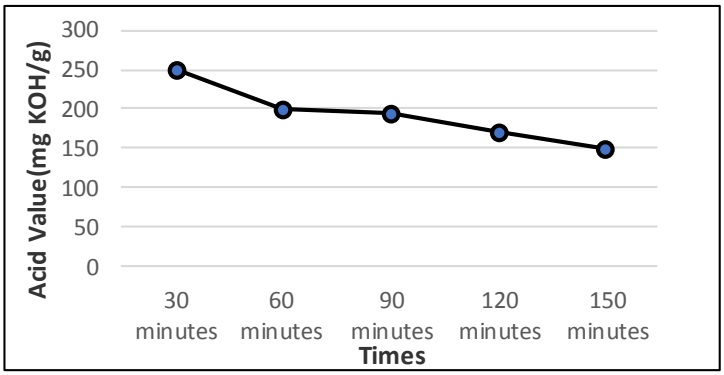

Figure 2: Graph of acid value for MSO sample

At 30 minutes of the synthesis, the acid value was 250mg KOH/g. It means that there is a lot of free fatty acid in the sample of MSO. When the synthesis continued for 1 hour, the acid value was high with 201mg KOH/g. There is 19.6% percentage different between 30 minutes and 1 hour of synthesis. Then, the acid value decreased a little to 195mg KOH/g at 1 hour and 30 minutes of synthesis. After that, it gradually dropped to 172mg KOH/g at 2 hours of synthesis. There is 11.8% percentage difference from the previous hour. Lastly, at the end of the synthesis, the acid value dropped to 150mg KOH/g and the percentage difference with previous acid value is 12.8%. When the acid value was low, there is small amount of free fatty acid content in the sample and it will have high amount of acid functionality due to the esterification process. Mazo *et al.*, (2011) reported that the decreasing of acid value was due to the reduction of the component's concentration. The component's concentration in this study referred to the free fatty acid.

CONCLUSIONS

In conclusion, maleinated resin from epoxidized soybean oil was successfully synthesized. The reduction in OOC and AV values indicate the formation of hydroxyl groups at the backbone of MSO.

The presence of ester group and disappearance of epoxy group in tryglycerides ESO backbone has been confirmed by AV and OOC test through wet titration. Hence, MSO can be further modified to produce MSO film coatings.

REFERENCES

Rucigaj, A., Alic, B., Krajnc, M., & Sebenik, U. (2014). Investigation of cure kinetics in a system with reactant evaporation: Epoxidized soybean oil and maleic anhydride case study. *European Polymer Journal*, 52, 105–116. doi.org/10.1016/j.eurpolymj.2014.01.009

Espana, J. M., Sánchez-Nacher, L., Boronat, T., Fombuena, V., & Balart, R. (2012). Properties of biobased epoxy resins from epoxidized soybean oil (ESBO) cured with maleic anhydride (MA). *Journal of the American Oil Chemists' Society*, 89(11), 2067–2075. Doi.org/10.1007/s11746-012-2102-2

Li, Y. T., Yang, L.T., Zhang, H., & Thang, Z., J. (2017). Synthesis and properties of a novel bio-based polymer from a modified soybean oil. *IOP Conference Series: Materials Science and Engineering, 170 012010.* doi:10.1088/1757-899X/170/1/012010

Liu, Z., Erhan, S. Z., & Xu, J. (2005). Preparation, characterization and mechanical properties of epoxidized soybean oil/clay nanocomposites. *Polymer*, 46(23), 10119–10127. doi.org/10.1016/j.polymer.2005.08.065

Mazo, P., Estenoz, D., Sponton, M., & Rios, L. (2012). Kinetics of the transesterification of castor oil with maleic anhydride using conventional and microwave heating. *Journal of the American Oil Chemists' Society*, 89, 1355-1361. https://doi.org/10.1007/s11746-012-2020-3

Keywords**:** *maleinated soybean oil, epoxidation, soybean oil, vegetable oil*

International Science, Technology and Engineering Conference, (ISTEC 2020) 42-44
e-isbn: 978 -967- 16937-1-1

FEASIBILITY OF BANANA PEELS AND SUGARCANE BAGASSE AS ECO-FRIENDLY LOST CIRCULATION MATERIAL ADDITIVES IN DRILLING MUD APPLICATION

Norizzatul Akmal Ismail Azhar[1], *Siti Khatijah Jamaludin[2], Arina Sauki[3], Dr. Hamizura Hassan[4] and Wan Ahmad Ilham Wan Mohamed Adnan[5]
[1,3,5] *Faculty of Chemical Engineering, Universiti Teknologi MARA, 40450 Shah Alam, Selangor, Malaysia*
[2,4] *Faculty of Chemical Engineering, Universiti Teknologi MARA, Cawangan Pulau Pinang, Permatang Pauh, 13500, Pulau Pinang, Malaysia*
*sitikhatijah@uitm.edu.my

PURPOSE/AIM & BACKGROUND

Loss circulation occurs when drilling fluid known as mud, flows into fractures of formations and not able to recirculate in oil and gas well during drilling process (Shaikh, 2010). The objectives of this paper are to conduct parametric study of banana peels and sugarcane bagasse as lost circulation material additive for drilling mud application and to investigate thermal stability of the formulated banana peels and sugarcane bagasse based lost circulation material. The performance of banana peel and sugarcane bagasse with different particle size were tested using Fann Viscometer and Low Pressure, Low Temperature (LPLT). The performance of the banana peels in rheological properties and filtration properties studies exhibited higher efficiency compared to the sugarcane bagasse and mud without LCM.

METHODOLOGY

Preparation of Banana Peels and Sugarcane Bagasse as potential LCM

These raw materials were cut into small pieces and dried for 2 days under sun to ensure no moisture content that may affect the efficiency of sample during experiment. Thereafter, samples were ground into smaller size and sieved by following the desired particle sizes; 0.3mm for fine, and 0.7 mm for coarse.

Mud Preparation

The water-based mud contained fresh water, sodium hydroxide, bentonite, xanthan gum and barite. Formulation A is a base fluid composition without LCM, whereas Formulation B is water-based mud with the environmentally friendly potential LCM which are banana peels and sugarcane bagasse.

Rheological Properties and Filtration Test Procedure.

In order to measure the plastic viscosity, gel strength, and yield point of drilling mud, Fann Viscometer was used in this test. Plastic viscosity functions to minimize high shear rate viscosity. Gel strength is important in order to classify the good mud formulation (Akeju, Akintola, & Akpabio, 2014). For Filtration Test, Low Pressure, Low Temperature (LPLT) Filter Press was used since these samples were tested at room temperature and pressure of 100psi. The filtration test will determine the amount of filtrate loss and mud cake thickness.

Thermal Stability Test

Fann Viscometer was set to three different temperature which are 25ºC, 50 ºC, and 100 ºC. Then, the best sample from previous test was tested again and the reading of plastic viscosity, gel strength and yield point was recorded and compared (Apaleke, Al-Majed, & Enamul, 2012).

FINDINGS/RESULTS

Rheological Properties Study.

Rheological properties on water-based mud analyzed were pH, mud weight, plastic viscosity (PV), yield point (YP), and gel strength (GS). All results were obtained using Fann Viscometer. The results

indicate that by having banana peels or sugarcane bagasse as additive in water-based mud, the rheological properties were altered. Banana peels and sugarcane bagasse additives enhance the value of plastic viscosity, yield point and gel strength of water-based mud compared to the blank sample which is the water-based mud sample without any additive.

pH and Mud Weight.

By adding banana peels, pH of the water-based mud changed to higher alkalinity and mud weight decreased. The blank sample can achieve up to 11ppg which is the standard mud weight that use in drilling industry. The eco-friendly LCM additives managed to reduce mud weight to the range of 8.9 – 9.9ppg. For sugarcane bagasse, value of alkalinity is higher compared to banana peels as additive.

Filtration Properties Study

Effect of Different Type of Raw Materials as Loss Circulation Materials.

The objective of this test is to observe the performance of water-based mud without LCM and with LCM in fluid lost controlling and formation of mud cake. Banana peels exhibited good performance in filtration compared to the sugarcane bagasse because the volume of filtrate in banana peel water-based formulation was less compared to sugarcane bagasse. Banana peels tends to give a significant result compared to sugarcane bagasse because it contains lignin, starch and cellulose, and is also fibrous.

Effect of Different Particle Size of Loss Circulation Materials.

A drilling fluid should contain particle size ranging up to the requisite maximum that should be able to effectively bridge the formation and form the filter cake (Alsaba, 2015). The smaller the particle size of drilling mud additives forms, the lower filtrate volume of drilling obtained. The fine sized of LCM has more surface area so they possess more resistance to pressure and they can plug more formation. For the mud cake thickness, the best range of mud cake thickness is between 2 to 25mm.

Thermal Stability Test for Loss Circulation Materials.

Banana peels with fine particle size and high concentration has been chosen as the optimum additives to prevent loss circulation materials. Therefore, this sample was used to complete the second objective of this study, which is to investigate the thermal stability of the optimum LCM. As the temperature increase up to 100 ºC, the rheological properties show the decreased pattern in the Fann viscometer reading. The reading of yield point at first temperature was 62kg/m^2 then decrease to 28 kg/m^2 and 25kg/m^2. Same goes to gel strength and plastic viscosity value decrease as well as the temperature increases. Temperature affects stability and resistant rheology of mud.

CONCLUSIONS

In conclusion, the important factor that can contribute to better performances of loss circulation material are particle size distribution and type of materials used. LCM with finer particle size is preferable compared to coarser LCM particle since finer size enhance filling behavior. By comparing all samples, Banana Peels produced better results compared to sugarcane bagasse as they have variety of crude fiber and the higher content of cellulose, lignin and starch. For the thermal stability study, when the temperature increases rapidly, the performance of rheological properties of banana peels degrade. At the same time, pH and mud weight of drilling mud are affected by using different type of additives. For recommendation, mud formulation can be improved by using different amount of additive. The mixing procedure also need to be modified such as integrating hot and cold rolling to make sure the mud and additives mix more perfectly.

REFERENCES

Akeju, O. A., Akintola, S. A., & Akpabio, J. U. (2014). The Use of Crassostrea Virginica as Lost Circulation Material in Water-Based Drilling Mud. *International Journal of Engineering and Technology,* 4(2), 109-117.

Alsaba, M. T. (2015). *Investigation of Lost Circulation Materials Impact on Fracture Gradient* (Doctoral Dissertations, Missouri University of Science and Technology, United States of America).
Retrieved from https://scholarsmine.mst.edu/doctoral_dissertations/2437

Apaleke, A. S., Al-Majed, A., & Hossain, M. E. (2012). Drilling Fluid: State of The Art and Future Trend. *Presentation at the North Africa Technical Conference and Exhibition,* Cairo, Egypt.

Retrieved from https://pdfs.semanticscholar.org/31b4/b1c7a206f6b53959e1799da4459815a8652c.pdf

Shaikh, A. M. (2010). *Environmental Management of Drilling Mud* (Masters thesis, Delft University of Technology, The Netherlands).
Retrieved from https://repository.tudelft.nl/islandora/object/uuid:a57fc0bc-ddc5-446c-9752-8f7d061df5e9/datastream/OBJ/download

***Keywords*:** Drilling Mud, Rheological Properties, Loss Circulation Material, Banana Peels and Sugarcane Bagasse

International Science, Technology and Engineering Conference, (ISTEC 2020) 45-47
e-isbn: 978 -967- 16937-1-1

ELECTRICAL PERFORMANCE OF $La_{0.6}Sr_{0.4}Co_{0.2}Fe_{0.8}O_{3-\delta}$ MODIFIED WITH LESS REDUCIBLE CATION

*Suhaida Dila Safian and Nafisah Osman
Faculty of Applied Sciences, Universiti Teknologi MARA, 02600 Arau, Perlis, Malaysia
*suhaidadila@uitm.edu.my

PURPOSE/AIM & BACKGROUND

Among the cathodes used for solid oxide fuel cells (SOFCs), $La_{0.6}Sr_{0.4}Co_{0.2}Fe_{0.8}O_{3-\delta}$ (LSFC) offer suitability for an intermediate temperature operation (600-800°C) due to its higher ionic and electronic conductivity than Lanthanum strontium manganite, LSM-based materials (Lanzini et al., 2009) . Besides that, at lower operation temperatures, LSCF are superior to LSM due to lower area specific resistance (ASR) value (Sun, Hui, & Roller, 2010). The successfulness of LSCF as mixed ionic or electronic conductor (MIEC) electrode is due to its high surface oxygen vacancy concentration at operating temperature, due to the replacement of Sr^{2+} dopant for La^{3+} host (Finsterbusch, Lussier, Schaefer, & Idzerda, 2012).

However, despite its outstanding advantages, the long-term stability of LSCF cathode as air-electrode has yet to be throughly verified experimentally. One of the concern of the issue is due to the cation segregation at the surface of perovskite oxides (Yu, Ludwig, Gopalan, Pal, & Basu, 2016). Recent study showed that perovskite-based electrode materials such as Sr^{2+}, Ba^{2+}, Pb^{2+} etc tends to segregate to the surface thus, formed an insulating resistive phase on the cathode surface. This significantly impacting the catalytic performance of the electrodes (Li et al., 2017). Furthermore, study showed that oxygen vacancies improve the diffusion process of oxygen species on the surface and in the lattice for oxygen reduction reaction (ORR), however it presence might also reduce the stability of the structure by increasing repulsive forces between atoms and weaken the attractive forces. Besides that, the increase in oxygen vacancies can also increase the probability of mechanical failure (Y. Wang, Duncan, Wachsman, & Ebrahimi, 2007).

Recently, there are substantial efforts in the research and development of LSCF based electrode material. The surface modification of LSC porous electrode has been claimed as a promising method to further improve the durability and enhanced the performance of SOFC (Tsvetkov, Lu, Sun, Crumlin, & Yildiz, 2016)(Jiang, 2019). Surface modification has been reported plays a key role in enhancing the ORR activity thus limiting pernicious cation segregation (H. Wang et al., 2019). İn this study, we modified the $La_{0.6}Sr_{0.4}Co_{0.2}Fe_{0.8}O_{3-\delta}$ (LSCF) film surfaces with a small amount of $ZrCl_4$ on the $Ba(Ce_{0.6}Zr_{0.4})_{0.9}Y_{0.1}O_{3-\delta}$ chemical bath deposition method.

METHODOLOGY

The LSCF powder as prepared elsewhere (Ismail, Jani, & Osman, 2017) was mixed with ethyle cellulose and terpinol to form cathode slurry then was spin coated on both sides of the BCZY pellet and fired at 600 ℃ and 950 ℃ respectively. A detail of BCZY pellet fabrication was previously reported elsewhere (Malaysiana, 2018)(Science, 2017). For the surface modification of LSCF, about 0.324 g of Zirconyl Chloride Octahydrate ($ZrOCl_2.8H_2O$) was dissolved in deionized water. The solution was stirred continuously and heat up to 80 ℃. The LSCF film was then submerged into the solution for 120 s and dried at 100 ℃ for 2 minutes.

The Electrochemical Impedance Spectroscopy (EIS) was carried out at 800 ℃ in the frequency range of 1 mHz to 1 MHz with 10 mV AC signal amplitude using ZIVE LAB wonATech. The spectrum curve fitting was performed using ZMAN™ 2.2 f3 (ZIVE LAB) software to analyze the impedance arcs referred to the equivalent circuits of four parallel pairs of R-CPE in series.

FINDINGS/RESULTS

Figure 1 shows the representative of the impedance spectrum recorded on the modified LSCF|BCZY|LSCF cell with platinum current collector at 800 °C in air. The spectrum was fitted with equivalent circuit of $Rs(R_1Q_1)(R_2Q_2)$ (Rahman et al., 2019), where Rs is the total Ohmic resistance and R_1Q_1 and R_2Q_2 correspond to the cathode processes (Ismail et al., 2017). İn the Nyquist plot, the high-frequency intercept of the impedance arc with real axis represents the ohmic resistance, Rs could be assigned to the contribution of the BCZY electrolyte as referred to the literature (Science, 2016).

The difference between the middle-low frequency intercepts indicate the polarization resistance, Rp which characterizes the electrode that associated with charge-transfer processes. This include oxygen ion diffusion in the cathode bulk and incorporation of oxygen ion from three-phase boundaries (Adler, Lane, & Steele, 1996). The polarization resistance (R_p) of the cathode is defined as the sum of R_1 and R_2, respectively. The area specific resistance (ASR) of the cathode is calculated using the relation $ASR = R_p \times S/2$ as S being the cathode surface area and factor ½ was applied due to the symmetrical cell used. The ASR obtained for modified LSCF-Zr^{4+} was 0.375 Ωcm^2 , remarkably lower than pristine LSCF value (1.01 Ωcm^2) reported by Ismail et al., (2017).

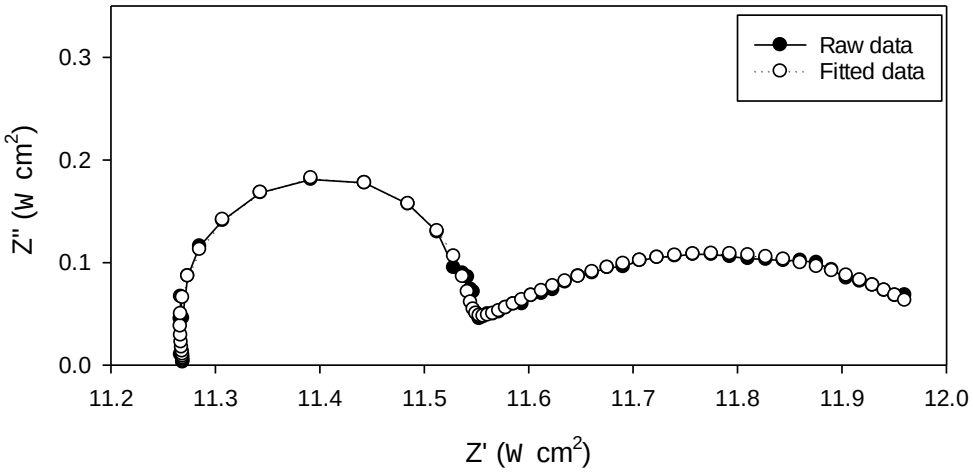

Figure 1: The electrochemical impedance spectrum of the modified symmetrical cell at θ = 800 ° in air

CONCLUSIONS

In conclusion, it is significantly showed that the surface modification of LSCF cathode system with less reducible cation has improved the electrical performance due to the Zr^{4+} metal cation enhanced the ORR activity. The evaluation on the electrochemical properties of the cathode in different type of atmospheres is in the progress and will be reported elsewhere.

ACKNOWLEDGEMENT

This research was supported by Ministry of Education (MOE) Malaysia via 600-IRMI/FRGS 5/3 (2017).

REFERENCES

Adler, S. B., Lane, J. A., & Steele, B. C. H. (1996). Electrode kinetics of porous mixed-conducting oxygen electrodes. *Journal of the Electrochemical Society*, *143*(11), 3554–3564. https://doi.org/10.1149/1.1837252

Finsterbusch, M., Lussier, A., Schaefer, J. A., & Idzerda, Y. U. (2012). Electrochemically driven cation segregation in the mixed conductor La 0.6 Sr 0.4 Co 0.2 Fe 0.8 O 3 - δ. *Solid State Ionics*, *212*, 77–80. https://doi.org/10.1016/j.ssi.2012.02.006

Ismail, I., Jani, A. M. M., & Osman, N. (2017). Microstructure control of SOFC cathode material: The role of dispersing agent. *AIP Conference Proceedings*, *1877*(September).

https://doi.org/10.1063/1.4999860
Jiang, S. P. (2019). Development of lanthanum strontium cobalt ferrite perovskite electrodes of solid oxide fuel cells – A review. *International Journal of Hydrogen Energy*, *44*(14), 7448–7493. https://doi.org/10.1016/j.ijhydene.2019.01.212
Lanzini, A., Leone, P., Santarelli, M., Asinari, P., Calì, M., & Borchiellini, R. (2009). Performances and Degradation Phenomena of Solid Oxide Anode Supported Cells With LSM and LSCF Cathodes: An Experimental Assessment. *Journal of Fuel Cell Science and Technology*, *6*(1), 011020. https://doi.org/10.1115/1.2971128
Li, Y., Zhang, W., Zheng, Y., Chen, J., Yu, B., Chen, Y., & Liu, M. (2017). Controlling cation segregation in perovskite-based electrodes for high electro-catalytic activity and durability. *Chem. Soc. Rev.*, *46*(20). https://doi.org/10.1039/C7CS00120G
Malaysiana, S. (2018). *as a Potential Cathode for Proton-Conducting Solid Oxide Fuel Cell*. *47*(2), 387–391.
Rahman, H. A., Ng, K. H., Ahmad, S., Taib, H., Mahzan, S., Salleh, S. M., … Muchtar, A. (2019). Influence of microstructure on the electrochemical behaviour of LSCF-SDCC. *IOP Conference Series: Materials Science and Engineering*, *494*(1). https://doi.org/10.1088/1757-899X/494/1/012062
Science, S. S. (2016). *Issn 0128-7389* |. *24*(2), 128–134.
Science, S. S. (2017). *Issn 0128-7389* |. *25*(1), 120–125.
Sun, C., Hui, R., & Roller, J. (2010). Cathode materials for solid oxide fuel cells: A review. *Journal of Solid State Electrochemistry*, *14*(7), 1125–1144. https://doi.org/10.1007/s10008-009-0932-0
Tsvetkov, N., Lu, Q., Sun, L., Crumlin, E. J., & Yildiz, B. (2016). Improved chemical and electrochemical stability of perovskite oxides with less reducible cations at the surface. *Nature Materials*, *15*(9), 1010–1016. https://doi.org/10.1038/nmat4659
Wang, H., Zhang, X., Zhang, W., Wei, Z., Guan, K., Meng, J., … Liu, X. (2019). Enhancing catalysis activity of La0.6Sr0.4Co0.8Fe0.2O3-Δ cathode for solid oxide fuel cell by a facile and efficient impregnation process. *International Journal of Hydrogen Energy*, *44*(26), 13757–13767. https://doi.org/10.1016/j.ijhydene.2019.03.184
Wang, Y., Duncan, K., Wachsman, E. D., & Ebrahimi, F. (2007). The effect of oxygen vacancy concentration on the elastic modulus of fluorite-structured oxides. *Solid State Ionics*, *178*(1–2), 53–58. https://doi.org/10.1016/j.ssi.2006.11.003
Yu, Y., Ludwig, K. F., Gopalan, S., Pal, U. B., & Basu, S. N. (2016). *Surface Segregation in Strontium Doped Lanthanum Cobalt Ferrite : Effect of Composition and Atmospheric Carbon Dioxide Surface Segregation in Strontium Doped Lanthanum Cobalt Ferrite : Effect of Composition and Atmospheric Carbon Dioxide*. 2–3.

Keywords: LSCF, surface modification;less reducible cation, Zr^{4+}, symmetrical cell, Area Specific Resistance

International Science, Technology and Engineering Conference, (ISTEC 2020) 48-50
e-isbn: 978 -967- 16937-1-1

OPTICAL, STRUCTURAL AND MORPHOLOGICAL PROPERTIES OF SiO_2-ZrO_2: Er^{3+}/Yb^{3+} THIN FILM DEPOSITED ON FUSED SILICA AND SILICON WAFER SUBSTRATE

Nurul Iznie Razaki, *Suraya Ahmad Kamil, Mohd Kamil Abd Rahman
School of Physics and Material Studies, Faculty of Applied Sciences, Universiti Teknologi MARA, 40450 Shah Alam, Selangor, MALAYSIA.
*suraya_ak@uitm.edu.my

PURPOSE/AIM & BACKGROUND

Rare earth (RE)-doped glasses have attracted interest among researchers since they have potential in numerous photonics applications such as in optical amplification (Kamil et al., 2016) lasing, color displays and imaging (Song, Chang, & Pecht, 2013). Among rare earth elements, Er^{3+} is known in optical signal amplification at 1.55 µm where this is coincides with the low-loss wavelength region of silica optical fibres. Er^{3+} transitions in blue, green and red spectral regions were also discovered to have potential in various applications (Kamil et al, 2019).

Er^{3+}-activated silica-zirconia (SiO_2-ZrO_2) thin film can be applied to produce optical amplifiers or lasers that can be integrated with other active or passive devices on the same chip. However, excess doping of Er^{3+} ion leads to quenching effect due to ion clustering. Yb^{3+} has strong absorption cross section about seven times larger than Er^{3+} at 980 nm wavelength. Thus, co-doping with Yb^{3+} would increase the pump rate, thus improve the emission intensity of the excited Er^{3+} ions inside the waveguides (Jha et al., 2012).

Incorporation of high RE ions dopant and usage of different type of substrate materials might affect the optical, structural and morphological properties of the resultant film**.** This paper attempts to prepare and characterize the glass ceramic thin film of $70SiO_2$- $30ZrO_2$:Er^{3+}/Yb^{3+}, deposited on fused SiO_2 substrate and silicon wafer via sol gel dip coating. Effects of the increment of the Er^{3+}/Yb^{3+} doping ratio and type of the substrate on the optical, structural and morphological properties of the deposited film were studied.

METHODOLOGY

The solution for film deposition was prepared by using sol gel technique and the film deposition on substrate (fused silica and silicon wafer) was carried out by computerized KSV dip coater system. The dipping and withdrawing speed were set up to 40 mm/min. The deposited film was annealed at 900°C layer by layer for 50 seconds. At final layer, the resultant film on the substrate was kept in tube furnace at 1000°C for 30 minutes for full film densification.

Thin film and refractive index measurements of these samples were measured by Prism coupler (SAIRON SPA 4000-R). Atomic force microscope (AFM XE-100 Park System (non-contact mode)) was employed to analyze morphology and surface roughness. Photoluminescence spectra and optical transparency were obtained using Horiba Jobin Yvon spectrophotometer (514.5 nm excitation of Argon ion) and UV -VIS-NIR spectrometer (Cary 5000 spectrophotometer Version 1.12), respectively. Raman spectroscopy (Raman Horiba Jobin Yvon Spectrometer) was used to determine the samples structural properties.

FINDINGS/RESULTS

Thin film samples coated on fused SiO_2 substrate demonstrate thickness from 3.09 µm to 3.30 µm and refractive indices value starting from 1.496 to 1.570. Meanwhile, the films coated on silicon wafer possess thicknesses ranging from 4.45 to 8.30 µm with the refractive indices value from 1.690 to 1.710. The film demonstrates full densification as the thickness decreases with increment of the refractive index. Film coated on silicon wafer has good adhesion as it demonstrates higher thickness compared to the film coated on the fused silica substrate. This might be due to the transformation of

the films structure, thus leads to volume expansion. It is believed that the orientation of the substrate surface influences the growth of the thin film as well as the nucleation sites.

From AFM, surface roughness of the film is decrease with addition of co-dopant Yb^{3+} until the doping ratio of Er^{3+}/Yb^{3+} reach to 1/10. At 1/5 (Er^{3+}/Yb^{3+}) doping proportion, the film demonstrates lowest surface roughness, for both substrate as the ions distributed homogeneously within the host matrix. It is believed that the Yb^{3+} co-dopant helps the ions distributed homogeneously inside the matrix thus promotes to smoother surface. The films deposited on silicon wafer exhibit smoother surface morphology compared to the deposited film on fused SiO_2 substrate as evidenced by low roughness value. The cleaning process of fused SiO_2 substrate contributes to the differences in the roughness of the resultant film. During the cleaning process, the surface condition of fused SiO_2 substrate is invisible. Presence of any contaminations would reduce adhesion of the first layer and the substrate, thus affect the roughness of the resultant film.

In photoluminescence spectra, Er^{3+} emissions both in green and red bands are decreased as the doping ratio of Er^{3+}/Yb^{3+} increased. Red emission peaks are more intense and narrower compared to the green. Domination of the red emission compared to the green might be due to the energy transfer from Er^{3+} to Yb^{3+}. In the presence of Yb^{3+}, the electrons from $^4S_{3/2}$ level transfer energy to the first excited state of Yb^{3+} thus depopulate the ions in the $^4S_{3/2}$ level of Er^{3+}. As a result, the green emission which originated from $^4S_{3/2}$ level of Er^{3+} is decreased.

The optical transmittance spectra of these thin films started to increase from 200 nm to NIR range with the percentage of 75% to 85%. High optical transparency indicates homogeneous and smooth film surface with small roughness (Cabello et al., 2010). From Raman spectra, samples with high content of ytterbium coated on both fused SiO_2 and silicon wafer exhibit broaden spectra. Meanwhile, sample with lower amount of co-dopant Yb^{3+} shows few weak peaks which attributed to SiO_2 network assigned by 400 cm^{-1}, 430 cm^{-1}, 1060 cm^{-1}, 1100 cm^{-1} (Ferrari et al., 2000; Marques & Almeida, 2006; Zampedri et al., 2004). It is believed that the co-dopant Yb^{3+} changes the structure of SiO_2-ZrO_2 matrix from crystalline to the amorphous phase. The addition of higher Yb^{3+} make the crystallization process less efficient as depicted by broaden band. Sharp and intense peak recorded at 550 cm^{-1} is due to silicon wafer used as the substrate. Besides that, the samples coated on these two different substrates with the similar doping ratio of Er^{3+}/ Yb^{3+} exhibit same pattern of spectra but differ in intensity. It can be concluded that having different substrate influenced crystallinity of the deposited materials.

CONCLUSIONS

Thin films coated on the silicon wafer showed positive influenced on the film properties compared to the fused silica substrate. Unlike fused SiO_2 substrate, silicon wafer has good orientation of the surface, therefore provide a good substrate or host for optical coating. This might also be attributed by cleaning process of the fused silica substrate. Contamination or unseen dust left on the uncoated substrate after the cleaning process may reduce the adhesion of the first layer on the substrate, thus affected the growth of the deposited film.

REFERENCES

Cabello, G., Lillo, L., Caro, C., Chornik, B., Soto, M. A., Del Río, R., & Tejos, M. (2010). Preparation and characterization of ZrO2:Sm amorphous thin films by solid state photochemical deposition method. *Journal of Physics and Chemistry of Solids*, *71*(9), 1367–1372. https://doi.org/10.1016/j.jpcs.2010.06.002

Ferrari, M., Armellini, C., Ronchin, S., Rolli, R., Duverger, C., Monteil, A., Innocenzi, P. (2000). Influence of the Er3+content on the luminescence properties and on the structure of Er_2O_3-SiO_2 xerogels. *Journal of Sol-Gel Science and Technology*, *19*, 569–572. https://doi.org/10.1023/A:1008701008906

Jha, A., Richards, B., Jose, G., Teddy-Fernandez, T., Joshi, P., Jiang, X., & Lousteau, J. (2012). Rare-earth ion doped TeO_2 and GeO_2 glasses as laser materials. *Progress in Materials Science*, *57*, 1426–1491. https://doi.org/10.1016/j.pmatsci.2012.04.003

Kamil, S. A., Zulkepli, N., Nawi, I. N. M., Razaki, N. I., & Rahman, M. K. A. (2019). Optical and Structural Properties of Er^{3+}-doped SiO_2-ZrO_2 Glass-Ceramic Thin Film. *Journal of Physics: Conference Series*, *1349*(1), 012035. https://doi.org/10.1088/1742-6596/1349/1/012035

Kamil, Suraya Ahmad, Chandrappan, J., Murray, M., Steenson, P., Krauss, T. F., & Jose, G. (2016). Ultrafast laser plasma doping of Er^{3+} ions in silica-on-silicon for optical waveguiding applications. *Optics Letters*, *41*(20), 4684–4687. https://doi.org/10.1364/OL.41.004684

Marques, A. C., & Almeida, R. M. (2006). Raman spectra and structure of multicomponent oxide planar waveguides prepared by sol-gel. *Journal of Sol-Gel Science and Technology*, *40*, 371–378. https://doi.org/10.1007/s10971-006-9320-8

Song, X., Chang, M. H., & Pecht, M. (2013). Rare-earth elements in lighting and optical applications and their recycling. *Journal of the Minerals, Metals and Materials Society*, *65*(10), 1276–1282. https://doi.org/10.1007/s11837-013-0737-6

Zampedri, L., Righini, G. C., Portales, H., Pelli, S., Nunzi Conti, G., Montagna, M., Armellini, C. (2004). Sol–gel-derived Er-activated SiO_2–HfO_2 planar waveguides for 1.5μm application. *Journal of Non-Crystalline Solids*, *345–346*, 580–584. https://doi.org/10.1016/j.jnoncrysol.2004.08.088

Keywords**:** *rare earth, Er^{3+}-doped, substrate, thin film, silica-zirconia*

International Science, Technology and Engineering Conference, (ISTEC 2020) 51-53
e-isbn: 978 -967- 16937-1-1

REMOVAL OF LEAD FROM AQUEOUS SOLUTION by TREATED SUGARCANE BAGASSE

Syarifah Nursyimi Azlina Syed Ismail, *Siti Najeehah Julkefli and Wahida Abdul Rahman
Universiti Teknologi Mara, Kampus Arau, 02600 Arau Perlis
*sitinajeehah2604@gmail.com

PURPOSE/AIM & BACKGROUND

Lead is one of the heavy metals that can be leached into the drinking water supply through corroded lead pipes, faucets and solder. It can give bad effects on human, animals, aquatic lives and plants. Most adsorbent that has been used is activated carbon due to its efficiency in adsorbing the element that are targeted. However, the problem rises as the cost for commercially activated carbon are high. The studies showed that agricultural waste can be used as adsorbent in removing heavy metal in wastewater. Agricultural waste like sugarcane bagasse is easy to get. Furthermore, it can minimize the impact of the abundance of sugarcane bagasse caused by business in selling sugarcane juice. Surface modification of the sugarcane bagasse can increase the active sites on the fibre of sugarcane bagasse at the same time eliminate all soluble components of sugarcane bagasse such as tannins, resins, reducing sugar, and colouring agents (Martín-Lara, et al., 2010). Polysaccharides in sugarcane bagasse contain abundance of hydroxyl and phenolic groups that have potential as a new compound after surface modification (Chand et al., 2015). High amount of cellulose, hemicellulose and lignin also has potential to achieve high adsorption of lead (Hegazi, 2013). Therefore, the objective of this study was to modify the sugarcane bagasse by using H_2SO_4 to produce chemically reactive surface for adsorption of lead (II). The adsorption performance of treated sugarcane bagasse, the effect of lead (II) concentration and the effect of adsorbent dosage were observed. Treated sugarcane bagasse showed better performance in adsorption of lead compared to untreated sample. The results indicated that the higher the dosage of adsorbent, the higher the adsorption percentages of lead. The lower the lead concentration, the higher the adsorption percentages by adsorbent.

METHODOLOGY

Treated Sugarcane bagasse

Sugarcane bagasse were washed and dried in the oven at 70ºC for 24 hours. Then, it was grinded to fine powder and sieved in the size of 150 µm. The powder sugarcane bagasse was immersed in concentrated sulphuric acid and heated at 150ºC. Then, it was immersed in diluted sodium hydroxide until the residual acid was removed. The material was dried in the oven for 24 hours at 150 ºC before further analysis.

Preparation of Adsorbate

Serial dilution of lead was made for 5ppm, 10ppm, 15ppm and 20 ppm.

Method of Adsorption

50 ml of lead solution of known concentration was added to 0.4 g of adsorbents in centrifuge tube. This was done at constant room temperature (29±ºC) and pH 7. The mixture was stirred and separated by filtering using filter paper. Then, the concentration of the sample was measured using ICP-OES to determine the concentration before and after the adsorption. The concentration of the adsorbate and the dosage adsorbent was varied to study the effect and performance of the adsorption. The sample from the experiment was run using ICP-OES to detect the concentration of the adsorbate before and after the adsorption.

Varying the Lead (II) Concentration

The lead concentration was varied by 5ppm, 10ppm, 15ppm, and 20 ppm and the adsorbent dosage was kept constant 0.4 g. The pH at 7 and 29±°C at room temperature. The time interval was 10, 20, 30, 40, 50 minutes.

Varying the Adsorbent Dosage

The experiment was done by changing the adsorbent dosage by 0.2g, 0.4g, 0.6g, 0.8g and 1.0g at constant concentration of lead (10 ppm) with pH 7.0 and 29±ºC at room temperature. The contact time are 10, 20, 30, 40, 50 minutes.

FINDINGS/RESULTS

The Effect of Lead (II) Concentration

The results for treated adsorbent have shown in figure 1. The graph in figure 1 has shown the increment of the percent of adsorption as the contact time increased with lower lead concentration. This is support by Tran et. al. (2017) which stated that the lower the lead concentration, the higher the percent of adsorption. This due to the low amount of metal ions in the solution making the adsorption of metal onto the surface of adsorbent almost 100%. The size of the porous structure also plays a role in the adsorption performance of sugarcane bagasse. The smaller the size, the higher the adsorption. The treatment with acid can changed porous of adsorbent form macrospores to microspores that indicate higher active sites produced and more efficient adsorption. Hence, at 150µm to 200 µm, the porous in the sugarcane bagasse functioning at its fullest in adsorbing the metal ion, in trends with the previous study by Joseph et al. (2009) and Pham et al. (2015). The graph of the percent of adsorption for treated sugarcane has increment starting from 10 minutes and becoming equilibrium from 20 minutes to 50 minutes. The equilibrium achieved indicated that the active site of the adsorbent has fully occupied thus the adsorption become equilibrium.

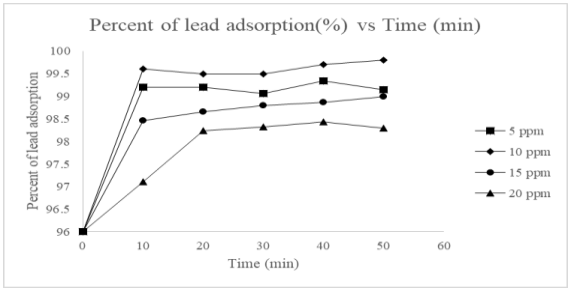

Figure 1: Effect of lead (II) concentration for treated sugarcane bagasse

The Effect of Adsorbent Dosage

The effect of adsorbent dosage for treated sugarcane bagasse has shown in figure 2. The percent of adsorption of lead increased gradually when the dosage of adsorbent increased. The percent increase from 58.30% to 99.30% at dosage of 0.2 g to 1.0 g. The lowest adsorption for treated sugarcane bagasse is 88.30% at 0.2 g of adsorbent. The highest is 99.30% which is at dosage of 1.0 g. When the adsorbents dosage increased, the surface area available for the adsorption of lead (II) ions also increased (Salihi et al., 2015). The graph has shown that there is an increment between 10 to 20 minutes before it reached equilibrium at 30 to 50 minutes. The equilibrium reached due to the surface of the sugarcane bagasse are completely occupied by the metal ions. This is in trend with the previous research by Salihi et al., (2015).

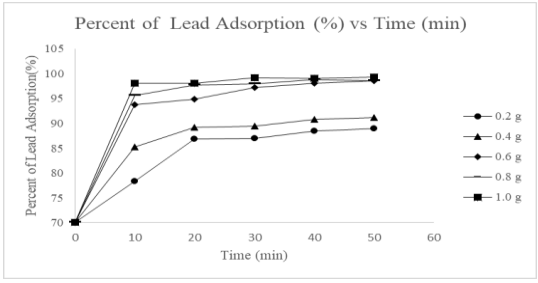

Figure 2: effect of adsorbent dosage for treated sugarcane bagasse

The Effect of Contact Time between Adsorbate and Adsorbent

The contact time was evaluated by varying the time (10, 20, 30, 40 and 50 minutes). For each 10-minute interval, the samples were collected for three times. The ideal time for the adsorption is at 50 minutes. The adsorption of lead by treated sugarcane bagasse occurs at fast rate. At 10 minutes, the

adsorption for treated sugarcane bagasse are increasing rapidly for all graph before it reached equilibrium. Short time are required to adsorb lead (II) ions due to the high propensity of carboxyl acid groups and ester group to form complexes with lead (II) ions (Shiralipour et al., 2018). At 40 to 50 minutes the graph increased gradually.

CONCLUSIONS

The performance of the adsorption by sugarcane bagasse are highly depends on the concentration of adsorbate and the adsorbent dosage. The higher the adsorbate concentration, the higher the percent of adsorption. For the case of adsorbent dosage, the higher the dosage, the higher the adsorption. The contact time for both conditions are varied. The contact time for the rate of adsorption in for the factor of concentration of lead are fast with 99.80% at 10 minutes. Meanwhile, for the adsorbent dosage the rate of adsorption is 66.50% at 50 minutes. Sulphuric acid work as chelating agents helps in producing more available chelating sites for removing of heavy metals.

REFERENCES

Tran V., T., Bui, Q. T. P., Nguyen, T. D., Le, N. T. H., & Bach, L. G. (2017). A comparative study on the removal efficiency of metal ions (Cu 2+ , Ni 2+ , and Pb 2+) using sugarcane bagasse-derived ZnCl 2 -activated carbon by the response surface methodology. *Adsorption Science and Technology*, *35*(1–2), 72–85. https://doi.org/10.1177/0263617416669152

Joseph, O., Rouez, M., Métivier-Pignon, H., Bayard, R., Emmanuel, E., & Gourdon, R. (2009). Adsorption of heavy metals on to sugar cane bagasse: Improvement of adsorption capacities due to anaerobic degradation of the biosorbent. *Environmental Technology*, *30*(13), 1371–1379. https://doi.org/10.1080/09593330903139520

Pham, T.T., Hoang, M.T., Nguyen, M.K., Dinh, T.H., Han, P.L., Bruggen, V.B. (2015). Evaluation of chemical modified sugarcane bagasse for cadmium removal in aqueous environment. *International Proceedings of Chemical, Biological and Environmental Engineering*, 88. doi: 10.7763/icpbee. 2015. V88. 2

Salihi, I. U., Kutty, S. R. M., Isa, M. H., Olisa, E., & Aminu, N. (2015). Adsorption of copper using modified and unmodified sugarcane bagasse. *International Journal of Applied Engineering Research*, *10*(19), 40434–40438.

Shiralipour, R., Hamoule, T., & Manochehripour, K. (2018). *Removal of Pb (II) From Contaminated Water by Bagasse Adsorbent Modified with Dithizone*. *10*(3). https://doi.org/10.5812/jjhs.62360.Research

Hegazi, H. A. (2013). Removal of heavy metals from wastewater using agricultural and industrial wastes as adsorbents. *HBRC Journal*, *9*(3), 276–282. https://doi.org/10.1016/j.hbrcj.2013.08.004

Chand, T. H., Raj, P. M., Nath, G. K., & Bahadur, K. D. (2015). *Removal of Arsenic from Aqueous Solution Using Iron (III) -loaded Sugarcane Bagasse Cellulose unit*. *5*(11), 51–58.

Martín-Lara, M. Á., Rico, I. L. R., Vicente, I. de la C. A., García, G. B., & de Hoces, M. C. (2010). Modification of the sorptive characteristics of sugarcane bagasse for removing lead from aqueous solutions. *Desalination*, *256*(1–3), 58–63. https://doi.org/10.1016/j.desal.2010.02.015

***Keywords*:** sugarcane bagasse, adsorbent, lead, water treatment, sulfuric acid

International Science, Technology and Engineering Conference, (ISTEC 2020) 54-56
e-isbn: 978 -967- 16937-1-1

PREPARATION AND CHARACTERIZATION OF *CAULERPA RACEMOSA* REINFORCED CORN STARCH BIODEGRADABLE FILM

[*]Wahida Abdul Rahman, Nur Badiah Raja Roslan, Noor Aishatun Majid and Syarifah Nursyimi Azlina Syed Ismail[3]
Faculty of Applied Sciences, UiTM Cawangan Perlis, Kampus Arau, 02600 Arau, Perlis,
[*]*wahida811@uitm.edu.my*

PURPOSE/AIM & BACKGROUND

The FTIR analysis, physical, mechanical and biodegradability properties of biodegradable blended film were characterized by using FTIR, solubility test, moisture uptake test, tensile test, and soil burial test. FTIR analysis confirmed the existence of good chemical interaction between (*Caulerpa Racemosa*) CR as filler and starch as matrix. The solubility and moisture uptake test revealed a slightly increasing trend when the composition of CR is more than 2.5%. When the composition of CR increased, the hydrophilic property of films increased due to large number of hydroxyl groups (OH) in the films. Therefore, the binding capability of hydroxyl group in film with hydroxyl group in moisture also increased. Tensile test result revealed that the increasing of CR composition had increased the flexibility and elasticity of the films produced. Films with 2.5% CR exhibit highest tensile strength and highest Young's modulus. Apart from that, soil burial test revealed that the increasing of CR compositions had increased the weight loss of film. Among the overall biodegradable blended films produced, film with 2.5% CR composition has been chosen as the best one due to good physical, mechanical and biodegradability properties. Thus, film with 2.5% CR may be the best option to produce biodegradable blended film with better properties. Therefore, different composition of seaweed and starch could be used to customize a film with desired application.

METHODOLOGY

Film Preparation

Solvent casting method was used to prepare the film. About 10 g corn starch was dissolved in 200 mL of distilled water and heated for 15 minutes at 60 °C with continues stirring. Raw CR with varies loading which were 0%, 2.5%, 5%, 10% and 15% were added into the solution. Then, 3 grams of glycerol was added and stirred the mixture with a constant temperature at 70 °C for two hours. The mixture was casted, cooled and dried at room temperature on glass plates (Agustin, 2014).

Film Characterization

The functional groups exists and compatibility of the CR filler and corn starch has been determined by using Fourier Transform Infrared Spectroscopy (FTIR) (Chong et al., 2018). Solubility test was conducted according to method by Moey, (2017). The moisture uptake of the films were determined by using method described by Tran et al., (2020). Mechanical properties of the film were determined by tensile test according to the method by Agustin et al., 2014. Biodegradability of the film were determined by using soil burial test method.

FINDINGS/RESULTS

The changes intensity of the peaks in the FTIR spectrum of film with different CR composition proven that the formation of new hydrogen bonding between starch and raw CR has taken place during the preparation of the blended film (Figure 1) (Jumaidin et al., 2017). The solubility test revealed that films with 2.5% and 10% CR exhibit lower solubility compare to other composition (Figure 2). This might be due to the higher water resistance of starch, which helps to prevent water absorption that can contribute to disintegration and dissolution (Jumaidin et al., 2017). Film with 2.5% CR exhibited the highest value for moisture uptake which can attribute to the highest number of exposed hydroxyl group existed in CR structure (Figure 2). Therefore, it can improve the binding capability of hydroxyl group in moisture with the hydroxyl group in CR structure. However, for CR composition of 15%,

10% and 5%, the moisture uptake reduces to 37.73%, 33.74, and 30.78% respectively. The declines can be due to the development of hydrogen bonding between the CR filler and the corn starch matrix hydroxyl functional group that reduces the moisture uptake of the films (D. Hermawan et al., 2019). Tensile test result revealed that the increasing of CR composition had increased the flexibility and elasticity of the films produced. Films with 2.5% CR exhibit highest tensile strength and highest Young's modulus. This phenomenon may be contributed as similar hydrophilic character of seaweed and starch matrix has resulted in good compatibility between them, promoting good material adhesion (Jumaidin et al., 2017). Soil burial test revealed that the increasing of CR compositions had increased the weight loss of film. Among the overall biodegradable blended films produced, film with 2.5% CR composition has been chosen as the best one due to good physical, mechanical and biodegradability properties. Thus, this film with 2.5% CR may be the best option for the desirable biodegradable blended film.

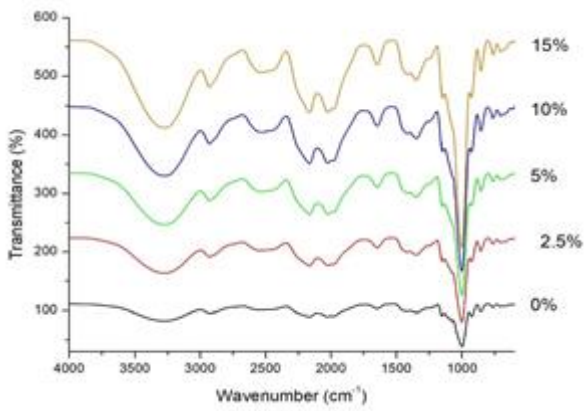

Figure 1: FTIR Spectrum of Film with Different Seaweed Composition

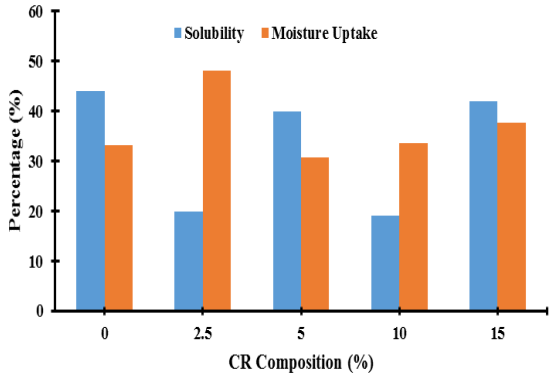

Figure 2: Solubility and moisture uptake for CR/corn starch blended film with different CR composition

CONCLUSIONS

In this study, the effect of different loading of raw *Caulerpa racemosa* (CR) seaweed on the functional group, physical, mechanical of the blended films were investigated. The addition of CR seaweed filler had a noticeable impact on the starch's physical, mechanical, and biodegradability. The increasing loading of seaweed filler in starch-based films showed significant increment of moisture uptake and solubility of the film. In addition, soil burial test indicates that the introduction of seaweed increases materials weight loss, indicating faster biodegradation of film. However, the value of tensile, elongation at break and young modulus decreased with the increased of seaweed content. The FTIR analysis results showed that good miscibility in blended film was due to the improved intermolecular interaction between CR seaweed and starch. From this study, the blended films with 2.5% raw *Caulerpa racemosa* came across as being the best physical, mechanical and biodegradability among all blended films.

REFERENCES

Abdul Khalil, H. P. S., Saurabh, C. K., Tye, Y. Y., Lai, T. K., Easa, A. M., Rosamah, E., Banerjee, A. (2017). Seaweed based sustainable films and composites for food and pharmaceutical applications: A review. *Renewable and Sustainable Energy Reviews*, *77*(September 2016), 353–362.

Afonso, C., Cardoso, C., Ripol, A., Varela, J., Quental-Ferreira, H., Pousão-Ferreira, P., Bandarra, N. M. (2018). Composition and bioaccessibility of elements in green seaweeds from fish pond aquaculture. *Food Research International*, *105*(August 2017), 271–277.

Agustin, M. (2014). Journal of Reinforced Bioplastic based on starch and cellulose nanocrystals from rice straw, (December).

Albano, C. (2005). rheological and toxicological behavior of HDPE / seaweed residues composites, *71*, 282–288.

Basha, K., & Rashid, A. (2018). Mechanical and thermal properties of starch films reinforced with, *2*(December), 555–563.

Chong, E. W. N., Abdul Khalil, H. P. S., Ying, T. Y., & Tajarudin, H. A. (2018). Preparation and characterization of red seaweed/calcium carbonate composite films. *IOP Conference Series: Materials Science and Engineering*, *368*(1).

D. Hermawan, J. Shima, A. Gopakumar, (2019). Development of Seaweed-based Bamboo Microcrystalline Cellulose Films Intended for Sustainable Food Packaging Applications, *14*, 3389–3410.

Siah, W. M., Aminah, A., & Ishak, A. (2015). Edible films from seaweed (Kappaphycus alvarezii). *International Food Research Journal*, *22*(6), 2230.

Tran, T. T. B., Roach, P., Nguyen, M. H., Pristijono, P., & Vuong, Q. V. (2020). Food Hydrocolloids Development of biodegradable fi lms based on seaweed polysaccharides and Gac pulp (Momordica cochinchinensis), the waste generated from Gac oil production. *Food Hydrocolloids*, *99*(August 2019), 105322.

Jumaidin, R., Sapuan, S. M., Jawaid, M., & Ishak, M. R. (2017a). International Journal of Biological Macromolecules Effect of seaweed on mechanical, thermal, and biodegradation properties of thermoplastic sugar palm starch / agar composites. *International Journal of Biological Macromolecules*, *99*, 265–273.

Keywords**:** *Caulerpa Racemosa*; FTIR; Young's Modulus; biodegradability; seaweed